ISBN: 978-0-12-391851-2

"**Ocean Circulation and Climate, 2nd Ed. A 21st century perspective**"

(Eds.): Siedler, G., Griffies, S., Gould, J. and Church, J.

Academic Press, 2013

Chapter 13 Western Boundary Currents

Shiro Imawaki[*]

Amy S. Bower[†]

Lisa Beal[‡]

Bo Qiu[§]

[*]Japan Agency for Marine–Earth Science and Technology, Yokohama, Japan

[†]Woods Hole Oceanographic Institution, Woods Hole, Massachusetts, USA

[‡]Rosenstiel School of Marine and Atmospheric Science, University of Miami, Miami, Florida, USA

[§]School of Ocean and Earth Science and Technology, University of Hawaii, Honolulu, Hawaii, USA

Abstract

Strong, persistent currents along the western boundaries of the world's major ocean basins are called "western boundary currents" (WBCs). This chapter describes the structure and dynamics of WBCs, their roles in basin-scale circulation, regional variability, and their influence on atmosphere and climate. WBCs are largely a manifestation of wind-driven circulation; they compensate the meridional Sverdrup transport induced by the winds over the ocean interior. Some WBCs also play a role in the global thermohaline circulation, through inter-gyre and inter-basin water exchanges. After separation from the boundary, most WBCs have zonal extensions, which exhibit high eddy kinetic energy due to flow instabilities, and large surface fluxes of heat and carbon dioxide. The WBCs described here in detail are the Gulf Stream, Brazil and Malvinas Currents in the Atlantic, the Somali and Agulhas Currents in the Indian, and the Kuroshio and East Australian Current in the Pacific Ocean.

Keywords

Western boundary current, Gulf Stream, Brazil Current, Agulhas Current, Kuroshio, East Australian Current, Subtropical gyre, Wind-driven circulation, Thermohaline circulation, Recirculation, Transport

1. General features

1.1. Introduction

Strong, persistent currents along the western boundaries of the world's major ocean basins are some of the most prominent features of ocean circulation. They are called "western boundary currents," hereafter abbreviated as WBCs. WBCs have aided humans traveling over long distances by ship, but have also claimed many lives due to their strong currents and associated extreme weather phenomena. They have been a major research area for many decades; Stommel (1965) wrote a textbook entitled *The Gulf Stream*: *A Physical and Dynamical Description*, and Stommel and Yoshida (1972) edited a comprehensive volume entitled *Kuroshio*: *Its Physical Aspects*, both milestones of WBC study. This chapter is devoted to describing the structure and dynamics of WBCs, as well as their roles in basin-scale circulation, regional variability, and their influence on atmosphere and climate. Deep WBCs are described only in relation to the upper-ocean WBCs.

A schematic global summary of major currents in the upper-ocean (Schmitz, 1996; Talley et al., 2011), spanning the depth interval from the sea surface through the main thermocline down to about 1000 m, is shown in Figure 1.6 in Chapter 1 (This figure will not appear in this chapter, but is shown in this preprint). Major WBCs are labeled as well as other currents. More detailed schematics of each WBC are shown in the following sections on individual oceans.

1.2. Wind-driven and thermohaline circulations

Anticyclonic subtropical gyres (red flow lines in Figure 1.6) dominate the circulation at midlatitudes in each of the five ocean basins. These gyres are primarily wind-driven, where the equatorward Sverdrup transport in the interior of each ocean, induced by the curl of the wind stress at the sea surface, is compensated by a strong poleward current at the western boundary (Stommel, 1948). Readers are referred to Huang (2010) and Chapter 11 for details on the physics of the wind-driven circulation, including WBCs. The poleward WBCs of these subtropical gyres are the Gulf Stream, Brazil Current, Agulhas Current, Kuroshio, and East Australian Current (EAC). These subtropical WBCs carry warm waters from low to high latitudes, thereby contributing to global meridional heat transport and moderation of Earth's climate. According to linear wind-driven ocean circulation

theory, WBCs separate from the western boundary at the latitude where the zonal integral of wind stress curl over the entire basin is zero. In fact, the dynamics of the separation process are very subtle, and actual separation latitudes are considerably lower than the latitude of zero wind stress curl, due to various details discussed in the following sections. The reproduction of WBC separation has been a benchmark of numerical models of general ocean circulation. After separation, the WBCs feed into the interior as meandering jets called WBC extensions.

Some WBCs also carry waters as part of the thermohaline circulation, involving inter-gyre and inter-basin exchanges as shown by green flow lines in Figure 1.6. For example, there is leakage via the Agulhas Current around the southern tip of Africa into the South Atlantic, the North Brazil Current affects cross-equatorial exchange from the South Atlantic into the North Atlantic, and the Gulf Stream and North Atlantic Current carry warm waters northward up into the Nordic Seas. Readers are referred to Chapter 11 for the thermohaline circulation and meridional overturning circulation (MOC), and Chapter 19 for inter-ocean and inter-basin water exchanges.

1.3. Transport

WBCs typically have widths of about 100 km, speeds of order 100 cm s^{-1}, and volume transports between 30 and 100 Sv (1 Sv = 10^6 m^3 s^{-1}). Their volume transport can be estimated as the compensation, at the western boundary, of the Sverdrup transport calculated from wind stress curl over the interior ocean. However, the local volume transport is usually larger than predicted by Sverdrup theory, due to a thermohaline component and/or lateral recirculations adjacent to the WBC.

Volume transports of most WBCs have an annual signal, which through Sverdrup theory corresponds to the annual cycle of wind stress curl over the interior ocean. However, the observed signal is considerably weaker than estimated from simple theory. This is thought to be due to the blocking of fast barotropic adjustment by ridge topography, while the baroclinic signal is too slow to transmit an annual cycle to the western boundary. A unique seasonality is observed in the volume transport of the Somali Current in the northern Indian Ocean, where the flow reverses annually with the reversal of the Asian monsoon winds. The Somali Current could not be classified as part of the subtropical gyre, but will be described in detail in the following sections, because of this uniqueness and its behavior extending into the subtropics.

1.4. Variability

Intrinsic baroclinic and barotropic instabilities of the WBCs result in meanders and ring shedding, and consequently, eddy kinetic energy (EKE) levels are elevated in WBC regions. Figure 13.1 shows the global distribution of climatological mean EKE (Ducet et al., 2000), estimated from almost 20 years of sea surface height (SSH) obtained by satellite altimeters, assuming geostrophic balance. The figure shows clearly that the EKE of WBCs and their extensions is much higher than in the interior. Especially, extensions of the Gulf Stream, Kuroshio, and Agulhas Current show very high EKE.

The EKE is also high in the transition from the Agulhas Current to its extension, located south of Africa. Another western boundary region of high eddy activity is located between Africa and Madagascar, caused by the Mozambique eddies, which replace the more standard continuous WBC there. EKE is enhanced at the western boundary of the northern Indian Ocean, due to the unique seasonal reversal of the Somali Current. See their details in the Indian Ocean section.

1.5. Structure of WBCs

WBCs have a baroclinic structure. This is illustrated for the Kuroshio south of Japan in Figure 13.2, which shows the vertical section of 2-year Eulerian-mean temperature and velocity during the World Ocean Circulation Experiment (WOCE). As in other WBCs, the flow is the strongest near the sea surface and decreases with depth. The velocity core, defined as the strongest along-stream flow at a given depth on a cross-stream vertical section, shifts offshore with increasing depth. Vertical and horizontal shears of the WBC are the strongest on the coastal (cyclonic) side, accompanying a strong gradient of sea surface temperature (SST). Geostrophic balance results in a SSH difference across a WBC of order 100 cm, with SSH higher on the offshore side (Figure 13.2b). The horizontal pressure gradient associated with this SSH difference is compensated by the baroclinic cross-stream pressure gradient associated with the main thermocline, which deepens by several hundred meters moving offshore across the current. As a result, the pressure gradient and velocity weaken with depth.

The SSH difference across a WBC has been found to be well correlated with its total volume transport, because the vertical structure is relatively stable and hence an

increase (decrease) of the total transport results from a proportional increase (decrease) of transport of each layer of the WBC (Imawaki et al., 2001). This relationship has been used to estimate a time series of Kuroshio transport from satellite altimetry data.

Despite high lateral velocity shears, WBCs inhibit cross-frontal mixing owing to the strong potential vorticity front across their flow axis and to kinematic steering (Bower et al., 1985; Beal et al., 2006). Figure 13.2c shows the potential vorticity front and its location relative to the velocity core in the case of the Kuroshio. The potential vorticity front is related to strongly sloping isopycnals and dramatic changes in layer depth across the current. Steering or trapping of particles results when the speed of the WBC is greater than the meander or eddy phase speeds. As a result, water masses at the same density can remain distinct within a WBC down to intermediate depths.

1.6. Air–sea fluxes

Midlatitude WBCs, and particularly their extensions, are regions of strong air–sea interaction, and therefore are important to Earth's climate (see Chapter 5). Figure 13.3a shows the global distribution of climatological mean net heat flux at the sea surface (Yu and Weller, 2007). The net heat flux is clearly the largest over the midlatitude WBCs, because warm water transported by the poleward WBCs from low to mid latitudes is cooled and evaporated by cold, dry continental air masses carried over the WBC regions by prevailing westerly winds. These large heat fluxes, together with moisture fluxes to the atmosphere and sharp SST fronts, contribute to the development of atmospheric disturbances. Recent studies show that storm tracks are found preferentially along WBCs and their extensions (e.g., Hoskins and Hodges, 2002; Nakamura and Shimpo, 2004; Nakamura et al., 2004, 2012), and effects of the sharp SST fronts can be detected even in the upper troposphere (e.g., Minobe et al., 2008).

Figure 13.3b shows the global distribution of the climatological mean flux of carbon dioxide (CO_2) from the ocean to the atmosphere (Takahashi et al., 2009). WBCs and their extension regions absorb large amounts of CO_2, because large wintertime heat loss leads to the formation of dense water, which is subducted into the interior ocean as a subsurface or intermediate mode water, carrying CO_2 away from the surface (Cronin et al., 2010). This is called a "physical pump." The "biological pump"

associated with spring blooms also plays an important role in the very large uptake of CO_2 in WBC regions (Ducklow et al., 2001).

1.7. Observations

Since WBCs are characterized by relatively small scales, high velocities, often large vertical extent, and energetic variability, observing and monitoring them is a challenging task. This challenge has attracted many inspired scientists and resourceful engineers to tackle the measurement of these highly energetic signals. However, none of the currently available technologies and methods can satisfy all the requirements for an observing system of high spatial and temporal resolutions (see Chapters 3 and 4). Therefore, merged hybrid approaches are required, using sets of coastal and offshore end-point moorings, reference moorings for surface flux, inverted echo sounders with pressure gauges, submarine cables, research vessels, ships of opportunity, neutrally buoyant floats, underwater gliders, etc. (Cronin et al., 2010; Send et al., 2010). On the basis of those observational data, numerical model studies, including data assimilation, contribute to further understanding of WBCs. For climate studies, long time series, including mooring arrays maintained for longer than 10 years, are needed, as well as sustained satellite observations of vector winds, SSH (altimetry), SST, and sea surface salinity.

1.8. WBCs of individual ocean basins

In the following sections, the features of major WBCs in different oceans are described in detail; we focus mostly on subtropical WBCs. They are the Gulf Stream System in the North Atlantic, the Brazil and Malvinas Currents in the South Atlantic, the Somali and Agulhas Currents in the Indian Ocean, the Kuroshio System in the North Pacific, and the EAC in the South Pacific (Figure 1.6).

2. North Atlantic

2.1. Introduction

The series of WBCs in the North Atlantic, collectively referred to here as the Gulf Stream System, have helped shape human history in the Western Hemisphere. Their swift surface currents influenced the expansion of European civilization toward North America, and the advection of warm subtropical waters to high northern latitudes profoundly impacts climate on both sides of the Atlantic. The Gulf Stream

System is also important on a global scale, being the primary conduit for the delivery of warm, saline waters to the Nordic and Labrador Seas, and therefore a central component of the global thermohaline circulation.

Several earlier works and reviews cover the classical ideas about WBC theory and observations in general, and the Gulf Stream specifically. Among these are Stommel's (1965) and Worthington's (1976) monographs, and Fofonoff's (1981) article in *Evolution of Physical Oceanography*. Schmitz and McCartney (1993) and Hogg and Johns (1995) summarize the observations up to the mid-1990s. Focus here will be mainly on recent (post-1995) advances in observation and understanding of low-frequency variability in the Gulf Stream System and its connection to the atmosphere, with some attention to earlier seminal contributions and some work that was not described in previous review articles.

The main components of the Gulf Stream System are shown in Figure 13.4. The first is the Florida Current, which originates where the Gulf of Mexico's Loop Current enters the Florida Straits. After leaving the confines of the Straits, the current is referred to as the Gulf Stream and continues northward along the continental shelf break of the eastern United States to the latitude of Cape Hatteras (35°N, 75°W). The current separates from the continental shelf near Cape Hatteras, flowing northeastward over the slope and into deepwater as a single free jet, the Gulf Stream Extension (GSE). Large-amplitude, propagating meanders develop along the GSE path—some of these meanders pinch off to form Warm (Cold) Core Rings north (south) of the mean path. The GSE is flanked by the cyclonic Northern Recirculation Gyre and anticyclonic Southern Recirculation Gyre (NRG and SRG). Near 40°N, 50°W, where the Grand Banks and Southeast Newfoundland Ridge extend southward into the abyssal plain, the GSE separates into several branches, including the recirculation return flows, the Azores Current, and the North Atlantic Current. The latter meanders northward off the eastern flanks of the Grand Banks and Flemish Cap to the so-called Northwest Corner near 52°N, where it turns abruptly eastward as a multibranched meandering flow toward the mid-Atlantic ridge.

2.2. Florida Current

The Florida Current is perhaps the most well-documented current in all the ocean basins. Its proximity to land and confinement within the Florida Straits (90 km wide, 700 m deep) have allowed frequent observations of its velocity structure and volume

transport using a variety of measurement techniques. By the early 1990s, the mean transport (about 32 Sv), a small but significant annual cycle in transport (with a summer maximum and a winter minimum and peak-to-peak range of 4–6 Sv), and the water mass composition (13 Sv of South Atlantic origin) were already well established (Niiler and Richardson, 1973; Larsen and Sanford, 1985; Lee et al., 1985; Molinari et al., 1985; Leaman et al., 1987; Schmitz and Richardson, 1991). The velocity structure is laterally asymmetric, with the mean surface velocity maximum of about 180 cm s^{-1} pressed up against the western boundary (Leaman et al., 1987; Beal et al., 2008). The current extends to the bottom of the channel with a mean velocity of about 10 cm s^{-1}. Most observational and model results point to local and regional wind stress variability as the cause of the annual cycle in transport (Anderson and Corry, 1985; Schott and Zantopp, 1985).

Of particular significance in the study of Florida Current variability has been the nearly continuous measurement of the daily transport at 27°N since 1982, based on the voltage difference across a succession of abandoned underwater telephone cables (Larsen, 1992). From the first 16 years of cable-derived transports, Baringer and Larsen (2001) confirmed earlier estimates of the mean transport as well as the amplitude and phasing of the annual cycle. But they also showed that the annual cycle weakened in the second half of the record. They further found that interannual transport variability was inversely correlated with the North Atlantic Oscillation (NAO) index (Hurrell, 1995), with the NAO leading Florida Current transport by about 18 months. This suggested a connection between wind stress variability over the North Atlantic subtropical gyre and transport in the Florida Straits.

Meinen et al. (2010) combine the cable-derived transport time series with other *in situ* transport estimates to produce a 40-year time series. They argued for caution when attempting to explain changes in the amplitude or phasing of the annual cycle, pointing out that the dominance of subannual transport variability (containing 70% of the total variance and caused by the frictional effect of fluctuating along-channel winds; Schott et al., 1988) can contaminate the annual cycle, which contains only about 10% of the total variance. On longer timescales, Meinen et al. (2010) showed that lagged correlation between Florida Current transport and the NAO index was statistically significant during 1982–1998, but not before or after that time period.

DiNezio et al. (2009) use 25 years of cable-derived Florida Current transport and wind fields from the NCEP (National Centers for Environmental Prediction)/NCAR

(National Center for Atmospheric Research) Reanalysis Project to examine the importance of wind stress curl variability over the North Atlantic to interannual transport variability in the Florida Current. They found that positive NAO index is associated with positive wind stress curl anomalies (contrary to what might be expected from a simple strengthening of the westerlies during the positive phase of the NAO), and a weakening of the southward Sverdrup circulation in the interior. This variability is correlated well with Florida Current transport at a lag of about half that predicted by classical baroclinic Rossby wave theory, and accounts for about 50% of the transport variability in the Florida Current. The faster baroclinic response time is consistent with some recent observational and theoretical studies that suggest that changes to the background potential vorticity distribution imposed by topography or the mean baroclinic circulation, or interaction with the atmosphere may speed up the westward propagation of long Rossby waves (see DiNezio et al., 2009 and references therein). DiNezio et al. (2009) also pointed out that other sources of Florida Current transport variability may lie upstream since nearly half of the transport is of South Atlantic origin.

2.3. Gulf Stream separation

At Cape Hatteras, the Gulf Stream separates from the edge of the continental shelf and flows obliquely across the slope into deepwater (Figure 13.4). Unlike some of the other major WBCs, the Gulf Stream separation latitude varies by less than ±50 km (Auer, 1987; Lee and Cornillon, 1995). The pioneering work on WBC separation based on idealized linear and nonlinear theory was focused primarily on the impact of wind stress patterns (Stommel, 1948; Munk, 1950; Munk et al., 1950; Charney, 1955). Since then, a number of other factors have been found to be important, including topography and adjacent currents; see Dengg et al. (1996) and Tansley and Marshall (2000) for reviews. For example, evidence is increasing that interaction of the GSE with the Deep Western Boundary Current (DWBC) and/or the NRG plays an important role. Several observational studies based on multiyear hydrography, velocity, and remote sensing records have revealed a correlation between north–south shifts in the GSE path northeast of Cape Hatteras and the strength of the southwestward flow in the NRG (Rossby and Benway, 2000; Rossby et al., 2005; Peña-Molino and Joyce, 2008). Some idealized modeling studies have also demonstrated how variability in the strength of the southwestward currents north of the GSE can impact the separation latitude (Thompson and Schmitz, 1989;

Ezer and Mellor, 1992; Spall, 1996a,b; Joyce et al., 2000; Zhang and Vallis, 2007). A common feature of the model Gulf Stream–DWBC crossover studies is that the DWBC apparently alters the background potential vorticity field and effectively isolates the overlying Gulf Stream from the sloping topography, thus allowing it to cross the continental slope with a minimum of vortex stretching.

Accurate simulation of Gulf Stream separation has been a benchmark for assessing the performance of numerical model simulations of North Atlantic general circulation; see review by Hecht and Smith (2008). Significant improvement was only achieved when computing resources were sufficient to resolve the radius of deformation for the first baroclinic mode with several model grid points (grid spacing of about 10 km or less) (Smith et al., 2000; Chassignet and Garraffo, 2001). However, Bryan et al. (2007) argued that a grid spacing less than 10 km is not sufficient to represent Gulf Stream separation and northward penetration of the North Atlantic Current east of the Grand Banks (Figure 13.4), an even more elusive feature in North Atlantic simulations. They showed that lower subgrid scale dissipation is also necessary, as this allows for a more energetic DWBC.

2.4. Gulf Stream Extension

After the Gulf Stream has left the constraint of the continental slope, it develops meanders in its path that grow to maximum amplitude around 65°W (e.g., Lee and Cornillon, 1995). This downstream widening of the meander envelope leads to some of the highest oceanic EKE levels, reaching maximum values near 3000 $cm^2\ s^{-2}$ at the sea surface (e.g., Fratantoni, 2001). Lee and Cornillon (1995, 1996a,b) provide a comprehensive description of the frequency–wave number spectrum of GSE meanders based on 8 years of Advanced Very High Resolution Radiometer (AVHRR) imagery. For more discussion of the dynamics of the subannual variability in the GSE path, including a review of intrinsic baroclinic and barotropic instability of the current, the reader is referred to Hogg and Johns (1995), Cronin and Watts (1996), and references therein.

Trajectories of hundreds of freely drifting, long-range subsurface floats (SOFAR: Sound Fixing And Ranging, and RAFOS: SOFAR spelled backward) have extended the remotely sensed view of the GSE to the thermocline level and deeper; see Davis and Zenk (2001) for a general review of Lagrangian techniques and observations in the ocean. Ocean eddies naturally disperse floats over large areas, making it possible

(with a sufficient number of trajectories) to map the horizontal structure of mean subsurface velocity and its variability over entire basins. This technique was used in several studies to reveal the horizontal structure of mean velocity of the GSE, the North Atlantic Current, and their adjacent recirculations (e.g., Owens, 1991; Carr and Rossby, 2000; Zhang et al., 2001b; Bower et al., 2002). Such direct measurement of the structure of the large-scale subsurface circulation is not readily achieved by any other means.

The GSE maintains a remarkably rigid baroclinic velocity structure even as its path undergoes large-amplitude meanders. This was first demonstrated by Halkin and Rossby (1985) at 73°W based on 16 sections of *absolute* velocity collected over 3 years with the Pegasus velocity profiler. After aligning all the sections in a stream-wise coordinate system (with the origin at the jet core), they found that two-thirds of the variability in the Eulerian frame was due to meandering of the GSE and not changes in the jet's velocity structure itself. Subsequent observational studies showed that the baroclinic velocity structure is more or less maintained as far east as 55°W, as shown in Figure 13.5 (Hogg, 1992; Johns et al., 1995; Sato and Rossby, 1995; Bower and Hogg, 1996). The constancy of the GSE's upper-ocean velocity structure has been further demonstrated recently by Rossby et al. (2010) based on a 17-year time series of weekly GSE crossings at 70°W by a container vessel, the *MV Oleander*, equipped with a hull-mounted acoustic Doppler current profiler (ADCP).

The inherently Lagrangian nature of float trajectories has been exploited to make inferences about the kinematics and dynamics of the GSE and North Atlantic Current. For example, Shaw and Rossby (1984) diagnosed the presence of significant vertical motions in the GSE based on the temperature change along the trajectories of 700 m SOFAR floats. Using isopycnal RAFOS floats, it was found that this vertical motion, as well as associated cross-stream exchange, is highly structured around GSE meanders, with upwelling in the thermocline approaching anticyclonic meander crests and vice versa moving toward cyclonic meander troughs (Bower and Rossby, 1989; Song and Rossby, 1995). This work led to a view of the GSE in the region of propagating meanders in which many fluid particles are constantly being expelled and replaced by others (Bower, 1991; Bower and Lozier, 1994; Lozier et al., 1996). A number of theoretical, numerical, and observational studies of fluid particle behavior in time-dependent jets followed (e.g., Samelson,

1992; Cushman-Roisin, 1993; Pratt et al., 1995; Duan and Wiggins, 1996; Lozier et al., 1997; Rypina et al., 2011).

The NRG and SRG are largely barotropic and swell the mean stream-wise transport of the GSE from 88 Sv just downstream of separation at 73°W (Halkin and Rossby, 1985), to 115 Sv at 68°W (Johns et al., 1995), and to a maximum of 150 Sv at 60°W (Hogg, 1992).

Several studies have used remote sensing observations to show that the mean path of the GSE is displaced 20–65 km farther north in fall compared to spring (Auer, 1987; Lee and Cornillon, 1995; Kelly et al., 1999). Based on 130 historical hydrographic sections across the GSE between Cape Hatteras and the New England Seamount Chain, Sato and Rossby (1995) found that the baroclinic transport in the upper 300 m also peaked in fall, when the path is at its northern extreme. However, baroclinic transport relative to 2000 m peaked in early summer and had peak-to-peak amplitude of 8 ± 3 Sv. They pointed out that the phasing of the annual cycle in the 0–2000 m transport is consistent with Worthington's (1976) hypothesis that winter convection in the SRG would deepen the thermocline and result in maximum transport in spring or early summer. However, they also showed that the downward displacement of isotherms occurred at depths below the depth of winter convection.

Kelly et al. (1999), using more than 4 years of altimetry-derived observations of the SSH difference across the GSE, found, like Sato and Rossby (1995), that the northerly fall position of the GSE was associated with an annual peak in surface geostrophic transport. They showed using historical hydrographic data that the seasonal change in surface transport was due to seasonal heating and was limited to the upper 250 m. The 17-year *MV Oleander* time series of upper-ocean transport shows a weak, surface-intensified annual cycle in layer transport with a maximum in mid-September, having amplitude of 4.3% of the mean at 55 m, and 1.5% at 205 m, compared to an average scatter around 1-year means of 15% (Rossby et al., 2010).

Some studies have shown that interannual-to-decadal variability in the GSE path is larger than the annual cycle, and is correlated with the NAO index. For example, Joyce et al. (2000) constructed a long time series of GSE position by using historical bathythermograph (BT) data over 35 years (1954–1989). They found significant correlation between the mean latitude of the GSE path and the NAO index, with the

GSE lagging by 1 year or less. Frankignoul et al. (2001) extended the scope of this study by analyzing 6 years of TOPEX/Poseidon altimetric data and 45 years of BT observations of subsurface temperature. They reported that the GSE was very far north during the TOPEX/Poseidon years due to an extended period of high positive NAO index. They concluded that the GSE responds passively to the NAO with a delay of 1 year or so, and that this relatively rapid response time is associated with NAO-related buoyancy fluxes over the recirculation gyres.

2.5. Air–sea interaction

A recent large, multiinstitutional program, called Climate Variability and Predictability (CLIVAR) Mode Water Dynamics Experiment (CLIMODE), has made considerable progress toward a better understanding of the influence of the Gulf Stream System on climate variability. Recent reviews cover the regional (Kelly et al., 2010) and basin-scale (Kwon et al., 2010) interactions between the atmosphere and the Gulf Stream System. Here a few of the major features are highlighted; the reader is referred to these review articles and the references therein for a more thorough discussion.

The Gulf Stream System, like most other WBCs, is a region of strong heat loss to the atmosphere. This is due in large part to advection of warm water to midlatitudes, where cold, dry continental air masses carried over the warm water by prevailing westerly winds generate elevated latent and sensible heat fluxes. The annual average net heat flux over the GSE reaches a maximum of nearly 200 W m^{-2} out of the ocean, the highest of any of the major WBCs (Yu and Weller, 2007; Figure 13.3a). On synoptic timescales, values of turbulent heat flux to the atmosphere as high as 1000 W m^{-2} have been recently observed using the direct covariance method (The Climode Group, 2009). This transfer of heat from the ocean to the atmosphere leads to a sharp drop in northward heat transport by the ocean at the latitude of Gulf Stream separation (see, e.g., Trenberth and Caron, 2001).

These air–sea heat fluxes and the large SST gradients associated with the Gulf Stream System contribute to localized development of extratropical disturbances, leading to a storm track that is anchored to the current's path (see, e.g., Hoskins and Hodges, 2002; Nakamura et al., 2004). Joyce et al. (2009) used 22 years (1983–2004) of daily air–sea fluxes and combined reanalysis/scatterometer wind fields along with subsurface temperature observations to show that regions of

maximum (2–8-day period) variance in latent and sensible heat flux, as well as meridional wind and wind divergence, all shifted in phase with north–south shifts in the GSE path.

While the impact of the Gulf Stream System on regional, near-surface atmospheric variability is becoming more clear (Kelly et al., 2010), the importance of WBCs in general, and the GSE specifically, to large-scale climate variability has been more difficult to unravel. A major step toward a better understanding was made by Minobe et al. (2008), who showed that the effects of the sharp SST gradient at the GSE can be detected in the upper troposphere. The annual climatology of upward motion from the European Center for Medium-Range Weather Forecasting (ECMWF) analyses is the strongest over the warm core of the GSE and extends into the upper troposphere (Figure 13.6a). Minobe et al. (2008) showed that this upward motion is associated with strong wind convergence at the sea surface (Figure 13.6a), and that the upper tropospheric divergence also tracks the path of the Gulf Stream and GSE in a climatological sense (Figure 13.6b). They went on to point out that the occurrence of cold cloud tops, indicative of high altitude, was elevated over the mean path of the Gulf Stream and GSE (Figure 13.6c). The full implications of such a connection between the lower and upper atmosphere over the Gulf Stream System on the large-scale atmospheric circulation are as yet unknown (Kwon et al., 2010).

2.6. North Atlantic Current

The North Atlantic Current extends to the highest latitude of any of the world's *subtropical* WBCs, about 52°N (Figure13.4). As such, it represents the continuation of northward heat transport that is part of the thermohaline circulation, and therefore, it is important to include in this review. Its velocity structure is similar to that of the GSE near 55°W; namely, it has significant baroclinic and barotropic velocity structure, although peak velocities in the upper-ocean are about half. The synoptic and time-mean North Atlantic Current both extend to the ~4000 m deep sea floor (Meinen and Watts, 2000; Fischer and Schott, 2002; Schott et al., 2004). As might be expected for such a deep-reaching current, the total mean northward volume transport by the North Atlantic Current is large, 140–150 Sv at 43°N (Meinen and Watts, 2000; Schott et al., 2004). Meinen and Watts (2000) argued that 50–60 Sv of this transport recirculates in the quasi-permanent anticyclonic Mann Eddy located at the offshore edge of the current (Mann, 1967), 86–96 Sv recirculates in a larger loop around the Newfoundland Basin, and only 30 Sv exits the basin to the east (Schmitz

and McCartney, 1993). There is some evidence for one or more branches leaving the North Atlantic Current at various latitudes along the flanks of the Grand Banks and Flemish Cap, and flowing eastward toward the mid-Atlantic ridge (Krauss et al., 1987); however, other studies show that most or all of the upper-ocean transport continues northward to the Northwest Corner near 52°W before turning eastward (Lazier, 1994; Pérez-Brunius et al., 2004a,b; Woityra and Rossby, 2008).

Historical hydrographic data, surface drifters, and subsurface floats have revealed that the North Atlantic Current generally follows the 4000 m isobath (Rossby, 1996; Kearns and Rossby, 1998; Carr and Rossby, 2000; Fratantoni, 2001; Zhang et al., 2001b; Bower et al., 2002; Orvik and Niiler, 2002). Unlike the propagating GSE meanders, North Atlantic Current meanders are largely locked to topographic features, including the Southeast Newfoundland Ridge, the Newfoundland Seamounts, and Flemish Cap (Carr and Rossby, 2000).

The penetration of the North Atlantic Current along the western boundary to the latitude of the Northwest Corner has been even more difficult to reproduce in ocean general circulation models than the Gulf Stream separation; some success has been achieved with model grid separation that resolves the first baroclinic Rossby radius at all latitudes (<10 km) and sufficiently low subgrid scale dissipation (Smith et al., 2000; Bryan et al., 2007). Lower resolution and/or higher viscosity suppress advection of warm water along the eastern flank of the Grand Banks, resulting in large SST and air–sea heat flux errors when compared to observations (Bryan et al., 2007). Even when the North Atlantic Current path is represented well, its volume transport in models is still too low by a factor of 2 (Bryan et al., 2007).

3. South Atlantic

3.1. Introduction

The major WBCs of the South Atlantic include the northward-flowing North Brazil Current (referred to as the North Brazil Undercurrent south of about 5°S; Stramma et al., 1995), the southward-flowing Brazil Current, and northward-flowing Malvinas Current (Figure 13.7). Although the North Brazil Current is considered to be the principle conduit for the flow of warm water into the North Atlantic in the upper arm of MOC, the focus in this chapter is on subtropical mostly and additionally subpolar, not tropical, WBCs. Comprehensive discussions of the western tropical South

Atlantic circulation can be found in Schott et al. (1998) and Johns et al. (1998).

3.2. Brazil Current

The origins of the Brazil Current are in the South Equatorial Current (SEC), the northern limb of the South Atlantic subtropical gyre (Figure 13.7). According to Peterson and Stramma (1991) and references therein, the SEC has two main branches: transport in the northern branch feeds the North Brazil Current and equatorial countercurrents, while the southern branch (~16 Sv) bifurcates at the western boundary, with most transport (12 Sv) supplementing the North Brazil Current and a smaller fraction (4 Sv) turning southward as the Brazil Current (Stramma et al., 1990). This bifurcation at the western boundary is typically located south of 10°S.

Knowledge of the volume transport of the Brazil Current and its low-frequency variability has suffered significantly from the lack of long-term, direct velocity observations, and by the fact that on the order of half of the total Brazil Current transport is over the continental shelf, where estimating currents from hydrography is less reliable (Peterson and Stramma, 1991). Geostrophic transport estimates of the Brazil Current from 12° to 25°S, relative to various intermediate levels of no motion, are all less than 11 Sv (Peterson and Stramma, 1991). The only transport estimate based on direct velocity measurements, made using the Pegasus profiler at 23°S, is 11 Sv southwestward, of which 5 Sv was estimated to be flowing over the shelf (Evans and Signorini, 1985). The Pegasus velocity profiles revealed a three-layer current structure, with the southward-flowing Brazil Current confined to the upper 400 m, overlying an intermediate northward flow with Antarctic Intermediate Water (AAIW) characteristics and a deep southward flow carrying North Atlantic Deep Water (NADW).

As the Brazil Current flows southward, it continues to hug the continental shelf break. Garfield (1990) used infrared imagery in the latitude range 21–35°S to show that the inshore edge of the current lies over the 200 m isobath on average, and is always inshore of the 2000 m isobath. South of 24°S, the Brazil Current geostrophic transport, defined as the southward flow of warm subtropical waters above about 400 m, increases to 20 Sv due to the influence of an anticyclonic recirculation cell adjacent to the Brazil Current (Garzoli, 1993). The 20 Sv is considerably less than the estimates of the interior northward Sverdrup transport, which vary from 30 to

60 Sv (Veronis, 1973, 1978; Hellerman and Rosenstein, 1983). Gordon and Greengrove (1986) suggested that the deficit in southward transport by the Brazil Current relative to the northward interior Sverdrup transport might be compensated for by the southward flow of NADW in the DWBC. Some studies have suggested, based on water mass characteristics, that AAIW flows southward, rather than northward, under the Brazil Current in this latitude range, leading to total geostrophic transports around 70–76 Sv at 37°S (McCartney and Zemba, 1988; Zemba and McCartney, 1988; Peterson, 1990).

3.3. Brazil Current separation and the Brazil–Malvinas Confluence

The Brazil Current separates from the western boundary where it meets the northward-flowing Malvinas (Falkland) Current, the subpolar WBC of the South Atlantic (Gordon and Greengrove, 1986; Olson et al., 1988). After colliding over the continental slope, both currents turn offshore and develop large-amplitude meanders and eddies (Figure 13.7). This highly energetic region is called the Brazil–Malvinas Confluence (hereafter the Confluence). Multiyear records of the Confluence latitude based on remote sensing observations show excursions of the WBC separation point along the western boundary as large as 900 km, with a mean latitude of separation at about 36–38°S (Olson et al., 1988; Peterson and Stramma, 1991; Goni and Wainer, 2001). This contrasts sharply with the more stable separation latitudes of the Gulf Stream and Kuroshio in the Northern Hemisphere (Olson et al., 1988). The mean separation/Confluence latitude is well north of the latitude of zero wind stress curl in the South Atlantic, 47–48°S (Hellerman and Rosenstein, 1983). Veronis (1973) speculated that the premature separation was related to the northward-flowing Malvinas Current, and Matano (1993) found support for this idea using analytical and numerical models.

Some of the separated Brazil Current flows generally southeastward, alongside the Malvinas Return Current, transporting relatively warm subtropical waters poleward to about 46°S at 53°W before turning back northeastward (Figure 13.7). This anticyclonic meander occasionally pinches off warm, saline eddies into the subantarctic region (see, e.g., Gordon, 1989).

3.4. Malvinas Current

The Malvinas Current, which originates as a branch of the Antarctic Circumpolar

Current, transports relatively cold, fresh subantarctic water northward along the 1000–1500 m isobaths of the Patagonian slope to the Confluence near 38°S (Figure 13.7). Spadone and Provost (2009) estimated a mean volume transport of 34.3 Sv based on 14 years of altimetric data “calibrated” with two independent periods of current-meter observations. It has been shown that relatively cold, fresh subpolar waters injected into the South Atlantic via the Malvinas Current can make their way to the Benguela Current system in the eastern South Atlantic, at times making up 50% of the waters transported northward in the upper limb of the MOC (Garzoli et al., 1997; Garzoli and Matano, 2011).

3.5. Annual and interannual variability

Significant annual cycles have been observed in Brazil and Malvinas Current transport and the latitude of the Confluence. Olson et al. (1988) used a multiyear record of AVHRR imagery and Geodetic Satellite (GEOSAT) altimetric data in the Confluence region to document an increase in Malvinas Current transport and a northward shift of the Confluence latitude during austral winter, and vice versa in summer. Witter and Gordon (1999) and Goni and Wainer (2001) used altimetric data to show that the annual and semi-annual signals account for most (up to 75%) of the observed variability in the position of the Confluence. Using 9 years of AVHRR images, Saraceno et al. (2004) argued that the latitude where the two currents collide is quite stable near 39.5°S, 53.5°W, but the orientation of the merged front swings from northeastward in winter to southeastward in summer, leading to a distinct seasonal cycle where the Confluence crosses the 1000 m isobath. Goni and Wainer (2001) further argued that the latitude of the Confluence is most sensitive to Brazil Current transport, and only correlated with Malvinas Current transport when Brazil Current transport is low.

An annual signal was also observed in Malvinas Current transport; but its amplitude exhibits strong interannual modulation. Spadone and Provost (2009) found very little energy at the annual period from 1993 to 2000; but after 2000 there was significant energy at the semi-annual and annual periods. Monthly mean transports for the whole record showed an annual peak of 37 Sv in July/August (austral winter).

Regarding variability at longer timescales, Witter and Gordon (1999) computed empirical orthogonal functions from 4 years of TOPEX/Poseidon altimetric data and

found significant interannual variability in the gyre scale circulation, characterized by zonal shifts in the center of the subtropical gyre and associated variations in the strength of the Brazil Current. The interannual changes in the subtropical gyre circulation were found to be correlated well with variations in the large-scale wind stress curl over the South Atlantic. Using 15 years of altimetric and surface drifter observations, Lumpkin and Garzoli (2011) documented a multiyear southward shift of the Confluence latitude at a rate of 0.6–0.9°decade^{-1} from 1992 to 2007. A comparable shift of the latitude of maximum wind stress curl averaged across the basin led the authors to conclude, like Garzoli and Giulivi (1994) and Witter and Gordon (1999), that the separation of the Brazil and Malvinas Currents from the western boundary is coupled to the basin-wide wind stress pattern on interannual-to-decadal, as well as annual, timescales. Using the latitude of maximum wind stress curl as a proxy for the Confluence latitude prior to 1992, Lumpkin and Garzoli (2011) went on to report a weak northward shift in the Confluence latitude from 1979 to 1992, suggesting that the shift observed from 1992 to 2007 may be part of a multidecadal oscillation.

4. Indian Ocean

4.1. Somali Current

4.1.1. Introduction

The Somali Current could be classified as part of the tropical gyre and therefore not a major WBC. However, because the Indian Ocean is cut off to the north by the Asian continent and the monsoon winds are so strong, the Somali Current extends into the subtropics and is worthy of inclusion here. In comparison to other WBC systems, there are sparse measurements of the Somali Current, particularly considering that its flow reverses seasonally with the reversal of the Asian monsoon winds. Only three coordinated occupations have been undertaken over the past 50 years. The International Indian Ocean Experiment during 1964–1966 resulted in Wyrtki's (1971) hydrographic atlas and a first look at the monsoon variability of the Somali Current (Swallow and Bruce, 1966). The Indian Ocean Experiment (INDEX) included a study of the Somali Current during the onset of the 1979 southwest monsoon (Leetmaa et al., 1982; Swallow et al., 1983). And in 1995 there were several crossings of the current during WOCE and Joint Global Ocean Flux Study (e.g., Beal and Chereskin, 2003). In addition, there have been moored arrays on the

equator and off the Horn of Africa and in the Socotra Passage (Schott et al., 1990, 1997). The circulation during the southwest monsoon is better measured and understood than that during the northeast monsoon. Little progress has been made in understanding the Somali Current over the past 10–15 years, mainly due to the dangers of Somali piracy, which continue to preclude *in situ* observations.

4.1.2. Origins and source waters

During the southwest monsoon, which peaks from July to September, the Somali Current flows northward from the equator up to the tip of the Arabian Basin at 25°N (Figures 13.8 and 13.9a). In contrast, during the northeast monsoon of December through February, the Somali Current flows (less strongly) southward between about 10°N and the equator (Figure 13.9b).

Throughout the southwest monsoon, the waters of the Somali Current largely originate in the SEC, flowing across the equator via the East African Coastal Current (EACC) (Schott et al., 1990). Therefore, water properties of the Somali Current include influence from the Indonesian Throughflow (Warren et al., 1966) and tropical surface waters, and are cooler and fresher than the interior of the Arabian Sea (Wyrtki, 1971). Surface water properties are also strongly influenced by evaporation and upwelling along the path of the monsoon jet, which follows the Somali coast and extends offshore from the Horn of Africa (Findlater, 1969). During the northeast monsoon, when the Somali Current flows to the south, it is partially fed by the North Monsoon Current, which flows westward across the Arabian Sea from the Bay of Bengal (Figure 13,9b). These waters are again fresher than the interior of the Arabian Sea. The annual mean Somali Current flows to the north since the southwest monsoon is stronger than its counterpart (Figure 13.9c).

4.1.3. Velocity and transport

The velocity structure of the summer Somali Current is understood to develop and deepen over the course of each southwest monsoon (Schott and McCreary, 2001), but there is an extreme degree of variability in both its strength and path on intraseasonal and interannual timescales (Luther, 1999; Wirth et al., 2002; Beal and Donohue, 2013). Weak northward flow is established in April, well before the onset of the southwest monsoon, by the arrival of annual Rossby waves at the western boundary (Brandt et al., 2002; Beal and Donohue, 2013). At the beginning of the

monsoon, the Somali Current is weak and shallow, and overlies a southward undercurrent (Quadfasel and Schott, 1982). At this time, the Somali Current is largely Ekman-driven, balanced by southward Ekman transport in the interior of the Arabian Sea, while the geostrophic flow is undeveloped (Hastenrath and Greischar, 1991; Beal et al., 2003). By the end of the season, the Somali Current can reach speeds of 350 cm s^{-1} at the surface and deepen to over 2000 m (Swallow and Bruce, 1966), resulting in a V-shaped structure similar to other WBCs (Beal and Chereskin, 2003). The transport has been measured to be as much as 70 Sv in late summer (Fischer et al., 1996) and is by then largely balanced by southward geostrophic transport in the interior (Beal et al., 2003). Less is understood about the development of the Somali Current in response to the northeast monsoon, although it is clearly weaker and shallower and almost purely Ekman-driven (Figure 13.9b; Hastenrath and Greischar, 1991). Volume transports are about 5–10 Sv (Quadfasel and Schott, 1983). A southward undercurrent appears to persist throughout the winter, connected to eastward undercurrents along the equator (Jensen, 1991). This undercurrent carries the Red Sea Water away from the Gulf of Aden (Schott and Fischer, 2000).

4.1.4. Separation from the western boundary

Unlike other steady WBCs, the Somali Current is associated with two quasi-stationary eddies that have coastal separations: the Southern Gyre and Great Whirl. The existence of these quasi-stationary eddies, rather than a continuous boundary current, has been shown to be the result of alongshore southwesterly winds and the slanted angle of the coastline, the latter arresting their northward migration (Cox, 1979; McCreary and Kundu, 1988).

The shallow (100 m deep) Southern Gyre is formed by the Somali Current separating from the coast at about 3°N and looping back across the equator (Düing et al., 1980; Jensen, 1991; Schott and McCreary, 2001). This circulation may result from an inertial overshoot of the EACC (Anderson and Moore, 1979), or from the local wind stress close to the equator which drives offshore currents (Cane, 1980). Monthly means from the global drifter climatology show that the Southern Gyre is a relatively short-lived feature and, on the decadal average, is an open loop that feeds into the South Equatorial Counter Current (SECC) (not shown).

Swallow et al. (1983) found that as the winds strengthen northward in June, the

Great Whirl spins up between 5° and 10°N (Schott and McCreary, 2001). Using a 3.5 layer model, Jensen (1991) suggests that the Great Whirl is formed by barotropic instability where the kinetic energy in the Somali Current is at a maximum and the gradient in relative vorticity is the largest. Its northern edge typically lies close to the axis of the monsoon jet, that is, the latitude of zero wind stress curl. Altimeter and drifter data show that there is weak anticyclonic flow, a precursor to the Great Whirl, as early as April, due to remote forcing, and that the Great Whirl typically remains until the beginning of November, more than a month after the monsoon winds are gone (Beal and Donohue, 2013).

A portion of the Somali Current continues northward through the Socotra Passage (off the Horn of Africa), across the mouth of the Gulf of Aden, and along the coast of Oman (Quadfasel and Schott, 1982; Schott et al., 1997) (Figure 13.9a), before a final, broad separation from the coast. Crossing the Gulf of Aden, the current can trigger or interact with eddies, which subsequently propagate westward toward the mouth of the Red Sea (Fratantoni et al., 2006; Al Saafani et al., 2007).

In the past, numerical experiments have suggested that the Southern Gyre migrates northward to coalesce with the Great Whirl toward the end of the southwest monsoon, and the circulation and Somali Current collapse. However, more recent higher resolution models (Wirth et al., 2002), and 18 years of satellite observations (Beal and Donohue, 2013) show that the Great Whirl is ringed by smaller cyclones 70% of the time and hence its variability and stability are dominated by mutual eddy advection. There appears to be no sequence of events attributed to the collapse of the circulation, other than an initiation by the change in wind forcing.

During the northeast monsoon, the Somali Current flows to the south and separates from the coast just south of the equator, where there is a confluence with the EACC. Both currents then feed into the SECC (Figure 13.9b).

4.1.5. WBC extension

The Somali Current does not have a recognized extension. During the southwest monsoon, the northern Somali Current, which flows through the Socotra Passage and along the coast of Oman, feeds gradually into the interior of the Arabian Sea between 15° and 25°N (Figure 13.9a). The curl of the wind stress vanishes at about 9°N, coincident with the northern arm of the Great Whirl.

4.1.6. Air–sea interaction and implications for climate

Much research on coupled modes over the Somali Current system relates to the effect of coastal upwelling cells inshore of the current to rainfall and wind anomalies. The relationship between the Somali Current and these upwelling cells is largely unexplored, although both will be weaker when monsoon winds are weaker.

A decrease in coastal upwelling strengthens monsoon rainfall over India by increasing SST and thus local evaporation and water vapor transport (Shukla, 1975; Izumo et al., 2008). Such a decrease has been related to weaker alongshore winds during monsoon onset, which are often related to El Niño conditions. In addition, coastal upwelling inshore of the Somali Current creates significant SST variability over small scales, which couples with variability in the monsoon jet, such that cool SSTs slow down local winds. This causes a feedback via local Ekman suction (pumping) downwind (upwind) of the SST anomaly, which tends to move the Ekman suction downwind (Halpern and Woiceshyn, 1999; Vecchi et al., 2004; Seo et al., 2008). Hence, air–sea coupling can feedback on the oceanic circulation.

On longer timescales, the Simple Ocean Data Assimilation reanalysis (Carton et al., 2000) shows that there may be a weakening trend in the Somali Current during 1950–1991, due to a decreasing cross-equatorial transport related to a trend in the reanalyzed winds (Schoenefeldt and Schott, 2006).

4.2. Agulhas Current

4.2.1. Introduction

The Agulhas Current is the WBC of the southern Indian Ocean subtropical gyre (Lutjeharms, 2006) and flows southwestward along the east coast of southern Africa between about 27° and 37°S (Figure 13.8). Its mean transport is 70 Sv at 32°S, making it the strongest WBC in either hemisphere at this latitude (Bryden et al., 2005). Once the Agulhas Current reaches the African cape, it separates and loops anticlockwise south of the continent to feed into the eastward Agulhas Return Current (Figure13.8). This loop, known as the Agulhas Retroflection, sheds rings, eddies, and filaments of Agulhas waters into the Atlantic down to depths of more than 2000 m (Gordon et al., 1992; Boebel et al., 2003; Van Aken et al., 2003). Estimates of this “Agulhas leakage” are highly uncertain, ranging from 2 to 15 Sv, with about four to six Agulhas Rings shed annually (de Ruijter et al., 1999;

Dencausse et al., 2010). Together with a leakage of waters south of Tasmania from the East Australia Current, which is described in the South Pacific section, Agulhas leakage forms the so-called Southern Hemisphere Supergyre, which links the subtropical gyres of the Pacific, Indian, and Atlantic Oceans (see Chapter 19).

More needs to be learned about the variability of the Agulhas Current and Retroflection, and especially about changes in leakage. On subseasonal timescales, variability of the current is dominated by four to five southward-propagating, solitary meanders per year (Grundlingh, 1979; Lutjeharms and Roberts, 1988; Bryden et al., 2005) (Figure13.10). There is no consensus on seasonality (Ffield et al., 1997; Matano et al., 2002; Dencausse et al., 2010), but variations in retroflection and ring-shedding have been related to El Niño/Southern Oscillation on interannual timescales (de Ruijter et al., 2004). For example, during an anomalous upstream retroflection coincident with La Niña (2000–2001), no Agulhas rings were shed for 5 months. On climate timescales, peaks in Agulhas leakage have been linked to glacial terminations (Peeters et al., 2004) and to the resumption of a stronger Atlantic MOC (Knorr and Lohmann, 2003) (Figure 13.11). A simulation of the twentieth century ocean suggests that Agulhas leakage is currently increasing under the influence of global climate change (Biastoch et al., 2009).

4.2.2. Origins and source waters

Waters of the Agulhas Current originate in the marginal seas of the northern Indian Ocean, in the Pacific, in the Southern Ocean, and within the subtropical gyre itself. To the north of the Agulhas Current, where the island of Madagascar shades the western boundary from the interior of the gyre, the poleward boundary flow is split into two: a direct route via the East Madagascar Current and a route via eddies advected through the Mozambique Channel (Figure 13.8). Long-term moorings show four or five large (350 km) anticyclonic eddies per year in the Mozambique Channel, carrying a mean southward transport of 17 Sv (Ridderinkhof et al., 2010). Relatively fresh waters from the Indonesian Throughflow and those formed in the high rainfall region along the equator (Tropical Surface Water), as well as salty waters at intermediate depth from the Red and Arabian Seas (Red Sea Water and Arabian Sea Low Oxygen Water), feed into the Agulhas Current mainly via these Mozambique eddies (Beal et al., 2006). Salty Subtropical Surface Water and waters subducted seasonally in the southeastern region of the gyre (South East Indian Subantarctic Mode Water; Hanawa and Talley, 2001) feed into the Agulhas Current mainly via the

East Madagascar Current. This current is less well measured than the Channel flow; at 20°S the geostrophic transport is estimated at 20 Sv (Donohue and Toole, 2003), while at the tip of Madagascar it is 35 Sv (Nauw et al., 2008). In addition to these boundary flow sources, a strong southwestern subgyre recirculates waters into the Agulhas Current (Stramma and Lutjeharms, 1997), including AAIW, which enters the Indian Ocean from the Southern Ocean at about 60°E (Fine, 1993). Finally, NADW is found everywhere below 2000 m within the Agulhas Current system, with 2 Sv flowing northeastward within the (leaky) Agulhas Undercurrent (Beal, 2009) and another 9 Sv flowing eastward with the Agulhas Return Current (Arhan et al., 2003).

4.2.3. Velocity and vorticity structure

The surface core of the Agulhas Current has maximum velocities over 200 cm s^{-1} and typically sits above the continental slope in over 1000 m water depth (Grundlingh, 1983). The vertical velocity structure is V-shaped, with the core of the current progressing offshore with depth such that the cross-stream scale of the flow (and geostrophic balance) is preserved (Figure 13.10b; Beal and Bryden, 1999). The Agulhas Current is more barotropic than the Gulf Stream, typically penetrating to the foot of the continental slope at 3000 m depth or more. Below about 1000 m, between the deep core of the Agulhas Current and the continental slope, the Agulhas Undercurrent flows in the opposite direction with speeds of 20–50 cm s^{-1} (Beal, 2009). Vertical and horizontal shears are at a maximum on the cyclonic, inshore side of the Agulhas Current, except within the undercurrent core, where shears are small. Comparisons of direct and geostrophic velocities have shown that the along-stream flow field (cross-stream momentum balance) is essentially geostrophic below 200 m (Beal and Bryden, 1999).

The velocity field of the Agulhas Current is highly variable, with a decorrelation timescale of 10 days in the along-stream component at 32°S (Bryden et al., 2005). The meander mode having a 50–70-day timescale dominates in both the Agulhas Current and Undercurrent velocity fields (Beal, 2009), and results from the growth of barotropic instabilities generated when anticyclones from the Mozambique Channel or dipoles from the East Madagascar Current interact with the mean flow field (Schouten et al., 2002; Tsugawa and Hasumi, 2010). A cross-section of an Agulhas Current meander is shown in Figure 13.10a.

The strongest potential vorticity gradients (>1.5 m^{-1} s^{-1} km^{-1}) in the Agulhas Current appear within the thermocline and just inshore of its velocity core. Here, relative vorticity contributes to the potential vorticity front, but layer depth changes dominate its structure (Beal and Bryden, 1999). The gradient of layer depth with offshore distance changes sign below the neutral density of 27.2 and this leads to weak potential vorticity gradients in the intermediate and deep layers. Hence, strong, cross-stream water-property gradients at these depths are largely due to kinematic steering (Bower et al., 1985; Beal et al., 2006), which maintains a separation between Tropical Surface Water and Red Sea Water inshore of the dynamical front, and Subtropical Surface Water and AAIW offshore.

4.2.4. Separation, retroflection, and leakage

The Agulhas Current separates from the African continent well before the latitude of zero wind stress curl, and subsequent to separation, there is retroflection and leakage. Early separation and leakage occur because the African cape lies north of the latitude of zero wind stress curl (and subtropical front, Figure 13.8), and hence there is a gap in the boundary through which Indo-Pacific waters can leak westward into the Atlantic. Retroflection occurs because the longitudinal slant of the African continental slope is westward, rather than eastward. This gives rise to southwestward flow at separation and the current must subsequently loop, or retroflect, back eastward to rejoin the Sverdrup gyre, as governed by the large-scale wind stress curl.

It is difficult to establish the mean geographical separation point of the Agulhas Current, since its path does not significantly diverge from that of the African continental slope until the latter ends at the tip of the Agulhas Bank. Theory suggests that the positions of separation and retroflection are linked and that they affect leakage. For example, separation will be farther to the northeast when Agulhas Current transport is greater, because isopycnal outcropping along the concave coastline will occur sooner (Ou and de Ruijter, 1986). In this case, the separated Agulhas Current has a more southward trajectory and greater inertia, and can attach more easily to the Agulhas Return Current with less leakage (van Sebille et al., 2009). Hence, in the absence of other far-field changes, a stronger Agulhas Current leads to less leakage and a more easterly (early) retroflection. Over the 20-year satellite record, the position of the retroflection has not varied greatly (Dencausse et al., 2010), perhaps because it is steered by the Agulhas Plateau, a

region of shallow topography southeast of the African cape (Speich et al., 2006). However, this inertial theory, together with variations in the wind field, is able to explain many of the paleoclimate observations of Agulhas leakage variability (Beal et al., 2011).

Retroflection of a WBC after separation is intrinsically unsteady and leads to the shedding of rings (Nof and Pichevin, 1996; Pichevin et al., 1999; van Leeuwen and de Ruijter, 2009). The spatial scale of Agulhas Rings (200–300 km) is much larger than mesoscale eddies (Schouten et al., 2000; van Aken et al., 2003), because they result from an unsteady flow (not an unstable flow) and their scale is governed by the flow-force, or momentum flux, of the outgoing Agulhas Return Current (Pichevin et al., 1999). These rings appear to carry most of the leakage of Agulhas waters into the Atlantic, with smaller cyclones, patches, and filaments carrying the rest (Richardson, 2007). The timing and frequency of Agulhas Rings have been related to various upstream processes, including the interaction of currents with Madagascar (Penven et al., 2006), the radiation of Rossby waves from the eastern boundary (Schouten et al., 2002), and the downstream propagation of instabilities (meanders and transport pulses) in the Agulhas Current (Lutjeharms and van Ballegooyen, 1988; Goni et al., 1997; Pichevin et al., 1999). However, it is unclear how these parameters are related to the strength of the Agulhas leakage, if at all. In a simulation of the twentieth century ocean with a nested, eddy-resolving Agulhas region, Biastoch et al. (2009) find that leakage increases significantly, while the number of rings is unchanged. Agulhas leakage is very difficult to measure in the real ocean because it is fundamentally a Lagrangian transport (van Sebille et al., 2010).

4.2.5. WBC extension

The extension of the Agulhas Current is the Agulhas Return Current (Figure 13.8), which flows eastward from the Agulhas Retroflection as a strongly barotropic current of width 60–80 km, with distinct water masses and a marked front separate from the subtropical front at least as far as 40°E (Read and Pollard, 1993). Its volume transport is over 100 Sv (including 9 Sv of NADW), reducing to about one quarter this strength upon reaching 76°E (Lutjeharms and Ansorge, 2001; Arhan et al., 2003). It is strongly meandering, with three quasi-stationary troughs (loops toward the equator) at the Agulhas Plateau, at 33°E, and at 39°E, with decreasing amplitude toward the east (Quartly and Srokosz, 1993; Boebel et al., 2003).

Cyclones are frequently shed from these troughs and propagate westward, sometimes to be reabsorbed by the adjacent trough.

4.2.6. Air–sea interaction

Latent and sensible heat fluxes increase three to five times over the warm waters of the Agulhas Current system and there is a deepening of the marine–atmospheric boundary layer, and increased formation of convective clouds (Jury and Walker, 1988; Lee-Thorp et al., 1998; Rouault et al., 2000). Over the Agulhas Return Current, the response of surface winds and sensible heat flux to SST fronts are almost twice as strong during austral winter than during summer (O'Neill et al., 2005). The Agulhas Current system influences storm track positions and storm development, as well as regional atmospheric circulation patterns (Reason, 2001; Nakamura and Shimpo, 2004), and has been linked to extreme rainfall events and tornadoes over southern Africa (Rouault et al., 2002).

Uniquely among WBCs, the Agulhas Current system is thought to be an important source of continental moisture (Gimeno et al., 2010). Rainfall over Africa is correlated with SST anomalies over the larger Agulhas Current system, which are associated with Indian Ocean Dipole and El Niño/Southern Oscillation cycles. Overall warming of the system since the 1970s may have increased the sensitivity of African rainfall to these cycles (Behera and Yamagata, 2001; Zinke et al., 2004).

4.2.7. Implications for climate

Paleoceanographic records and models have suggested links between Agulhas leakage strength and past climate change (Figure 13.11; Beal et al., 2011). In particular, an assemblage of planktonic foraminifera characteristic of modern-day Agulhas waters found in marine sediment records show that dramatic increases in Agulhas leakage have occurred at the onset of each glacial termination over the last 550,000 years (Peeters et al., 2004). Weaker Agulhas leakage is associated with glacial climate and appears to be correlated with a more northerly position of the subtropical front and a weaker Atlantic overturning circulation (Figure 13.11). Moreover, during the last deglaciation, the delay in and then abrupt warming of the North Atlantic (Bølling warm event) have been attributed to changes in Agulhas leakage through its influence on Atlantic overturning (Knorr and Lohmann, 2003; Chiessi et al., 2008).

Ocean and coupled model studies corroborate these climate data, showing that Agulhas leakage variability can impact Atlantic overturning on a number of timescales. Planetary waves associated with Agulhas Rings can cause small decadal oscillations in the overturning (Biastoch et al., 2008), and buoyancy forcing associated with the advection of saline Agulhas waters into the North Atlantic enhances deepwater formation (Weijer et al., 2002), strengthening the MOC 15–30 years after an increase in leakage. The Agulhas leakage strength is affected by changes in the strength and position of the southeast trade winds and/or Southern Hemisphere westerlies (de Ruijter, 1982; Biastoch et al., 2009; Sijp and England, 2009). In a warming climate, the westerlies shift poleward, increasing the gap between the African continent and the subtropical front, thereby increasing leakage (Beal et al., 2011). This ties with inertial theory as discussed previously (de Ruijter et al., 1999). A simulation of the twentieth century ocean (with a nested, eddy-resolving Agulhas region) shows that Agulhas leakage may be increasing now, under anthropogenic climate change (Biastoch et al., 2009), which could strengthen Atlantic overturning at a time when warming and fresh meltwater input in the North Atlantic are predicted to weaken it.

5. North Pacific

5.1. Upstream Kuroshio

The Kuroshio is the WBC of the wind-driven subtropical gyre in the North Pacific. Its origin can be traced back to the Philippine coast, where the westward-flowing North Equatorial Current (NEC) bifurcates (around 15°N) and has its northern limb feeding into the nascent Kuroshio (Nitani, 1972; see Figure 13.12a). This bifurcation, and hence the Kuroshio, tends to shift northward with increasing depth (Reid, 1997, see his figure 5), due to the ventilation of the wind-driven, baroclinic subtropical gyre (Pedlosky, 1996). On seasonal timescales, the Kuroshio east of the Philippine coast tends to migrate northward and have a smaller volume transport in winter (November/December), and to shift southward and have a larger transport in summer (June/July). On interannual timescales, the Kuroshio begins at a more northern latitude and has a weaker volume transport during El Niño years (e.g., Qiu and Lukas, 1996; Kim et al., 2004; Kashino et al., 2009; Qiu and Chen, 2010).

The Kuroshio becomes a more coherent and identifiable boundary jet downstream of the Luzon Strait at 22–24°N, east of Taiwan (e.g., Centurioni et al., 2004). This is in

part due to the addition of mass from the interior, wind-driven Sverdrup gyre. Moored current-meter observations show that the Kuroshio has a mean volume transport of 21.5 Sv east of Taiwan (Johns et al., 2001; Lee et al., 2001). The Kuroshio path and transport in the latitude band from 18° to 24°N are highly variable due to westward-propagating, energetic mesoscale eddies from the interior ocean (Zhang et al., 2001a; Gilson and Roemmich, 2002; see Figure 13.1). These impinging eddies have a dominant period of ~100 days and are generated along the North Pacific Subtropical Countercurrent (STCC) as a result of baroclinic instability between the surface eastward-flowing STCC and the subsurface westward-flowing NEC (Qiu, 1999; Roemmich and Gilson, 2001). Perturbations induced by these impinging eddies force part of the northward-flowing Kuroshio to divert to the east of the Ryukyu Island Chain from 24°N, 124°E to 28°N, 130°E, contributing to the formation of the Ryukyu Current (Ichikawa et al., 2004; Andres et al., 2008).

North of 24°N, the main body of the Kuroshio enters the East China Sea where the Kuroshio path is topographically steered by the steep continental slope and approximately follows the 200 m isobaths (e.g., Lie et al., 1998). From repeat hydrography, the mean Kuroshio transport across the PN section (PN stands for Pollution Nagasaki; nominally from 27.5°N, 128.25°E to 29°N, 126°E) is estimated at 23.7–25.0 Sv (Ichikawa and Beardsley, 1993; Kawabe, 1995). With the time-mean Sverdrup transport across 28°N estimated at ~45 Sv (Risien and Chelton, 2008), this suggests that only 53–55% of Sverdrup return flow is carried poleward by the Kuroshio inside the East China Sea. The remaining ~20 Sv are likely carried northward by the offshore Ryukyu Current, although this is yet to be confirmed observationally.

Shielded to the east by the Ryukyu Island Chain, the Kuroshio inside the East China Sea avoids the direct impact from the westward-propagating interior eddy perturbations. Instead, the Kuroshio variability along the continental shelf break here is dominated by frontal meanders that tend to originate northeast of Taiwan and grow rapidly in amplitude while propagating downstream. The frontal meanders have typical wavelengths of 100–350 km, wave periods of 10–20 days, and downstream phase speeds of 10–25 cm s^{-1} (Sugimoto et al., 1988; Qiu et al., 1990; Ichikawa and Beardsley, 1993; James et al., 1999). When reaching the Tokara Strait at 29°N, 130°E, the fully developed frontal meanders can result in lateral Kuroshio path fluctuations as large as 100 km (e.g., Kawabe, 1988; Feng et al., 2000). Based

on tide gauge measurements across the Tokara Strait, the Kuroshio transport has been inferred to reach a seasonal maximum in spring/summer and a minimum in fall. Interannually, the Kuroshio transport at the Tokara Strait is inferred to increase in the year preceding El Niño events and to drop significantly during the El Niño years (Kawabe, 1988).

5.2. Kuroshio south of Japan

Exiting from the Tokara Strait, the Kuroshio enters the deep Shikoku Basin, and its mean eastward volume transport increases to 52–57 Sv (Qiu and Joyce, 1992; Imawaki et al., 2001). This transport increase is due to both the confluence of the northward-flowing Ryukyu Current and the excitation of a southern recirculation gyre. Subtracting the contribution from the recirculation reduces the net eastward mean transport of the Kuroshio south of Japan to 34–42 Sv. Seasonally, the Kuroshio transport south of Japan varies by about 10 Sv, much smaller than the 40 Sv inferred from wind-driven Sverdrup theory (Isobe and Imawaki, 2002). Near 139°E, the Kuroshio encounters the meridionally oriented Izu Ridge that parallels 140°E south of Japan. Its presence restricts the Kuroshio from exiting the Shikoku Basin either near 34°N, where a deep passage exists, or south of 33°N, where the ridge height drops.

On interannual timescales, the Kuroshio in the Shikoku Basin is known for its bimodal path fluctuations between straight and meandering paths. In its “straight path,” the Kuroshio flows along the Japanese coast, while a “large meander path” signifies a curving, offshore path (Kawabe, 1995). In addition to these two paths, the Kuroshio also inhabits a third, relatively stable path that loops southward over the Izu Ridge. It is interesting to note that while the large meander path persisted for several years in the 1970s and 1980s, since the 1990s it has occurred only once in mid-2004 for a period of about 1 year. During the past two decades, the Kuroshio path south of Japan largely vacillated between the straight path and the third path, detouring over the Izu Ridge (e.g., Usui et al., 2008). Theoretical and modeling studies attempting to explain the multiple path state of the Kuroshio south of Japan have a long history. Relevant reviews and references can be found in Qiu and Miao (2000) and Tsujino et al. (2006). In addition to be important for fisheries south of Japan, the bimodal Kuroshio path fluctuations have recently been shown to impact on development and tracks of wintertime extratropical cyclones that pass over south of Japan (Nakamura et al., 2012).

5.3. Kuroshio Extension

After separating from the Japanese coast at 36°N, 141°E, the Kuroshio enters the open basin of the North Pacific, where it becomes the Kuroshio Extension (KE). The Kuroshio separation latitude is located to the south of the zero Sverdrup transport stream-function line at 40°N in the North Pacific (Risien and Chelton, 2008). This southerly separation of the Kuroshio is due to the combined effect of the coastal geometry of Japan and the inertial nature of the Kuroshio/KE jet (Hurlburt et al., 1996). Free from the constraint of coastal boundaries, the KE has been observed to be an eastward-flowing inertial jet accompanied by large-amplitude meanders and energetic pinched-off eddies (e.g., Mizuno and White, 1983; Yasuda et al., 1992). Compared to its upstream counterpart south of Japan, the KE is accompanied by a stronger southern recirculation gyre. A lowered-ADCP survey across the KE southeast of Japan revealed that the eastward volume transport reached 130 Sv, which is more than twice the maximum Sverdrup transport in the subtropical North Pacific (Wijffels et al., 1998). Recent profiling float and moored current-meter observations have further revealed the existence of a recirculation north of the KE jet with a transport of about 25 Sv (Qiu et al., 2008; Jayne et al., 2009).

In addition to the high level of mesoscale eddy variability, an important feature emerging from recent satellite altimeter measurements and eddy-resolving ocean model simulations is that the KE system exhibits clearly defined decadal modulations between a stable and an unstable dynamic state (Vivier et al., 2002; Qiu and Chen, 2005; Taguchi et al., 2007). Figure 13.13 shows that the KE paths were relatively stable in 1993–1995, 2002–2005, and 2010. In contrast, spatially convoluted paths prevailed in 1996–2001 and 2006–2009. These changes in path stability are merely one manifestation of the decadally modulating KE system. When the KE jet is in a stable dynamic state, available satellite altimeter data further reveal that its eastward transport and latitudinal position tend to be greater and more northerly, its southern recirculation gyre tends to strengthen, and the regional EKE level tends to decrease. The reverse is true when the KE jet switches to an unstable dynamic state.

Transitions between the two dynamic states of KE are caused by the basin-scale wind stress curl forcing in the eastern North Pacific related to the Pacific decadal oscillations (PDOs) (Qiu and Chen, 2005; Taguchi et al., 2007). Specifically, when the central North Pacific wind stress curl anomalies are positive (i.e., positive PDO

phase; see Figure 13.14), enhanced Ekman flux divergence generates negative local SSH anomalies. As these wind-induced negative SSH anomalies propagate westward into the KE region after a delay of 3–4 years, they weaken the zonal KE jet, leading to an unstable state of the KE system with a reduced recirculation gyre and an active EKE field. The negative, anomalous wind stress curl forcing during the negative PDO phase, on the other hand, generates positive SSH anomalies through the Ekman flux convergence. After propagating into the KE region in the west, these anomalies stabilize the KE system by increasing the KE transport and by shifting its position northward.

Decadal modulations in the dynamic state of KE can exert a significant impact on regional water mass formation and transformation processes. During the unstable state of the KE system, for example, the elevated eddy variability brings upper-ocean high potential vorticity water of the Mixed Water Region southward, creating a stratified upper-ocean condition in the southern recirculation gyre region, which is unfavorable for the wintertime deep convection and Subtropical Mode Water (STMW) formation (Qiu et al., 2007a; Sugimoto and Hanawa, 2010). In addition, changes in the dynamic state of KE are also important for the evolution of formed STMW. While it tends to remain trapped within the recirculation gyre during the unstable state of the KE jet, STMW tends to be carried away from its formation region during the stable state of KE (Oka, 2009; Oka et al., 2011).

By transporting warmer tropical water to the midlatitude ocean, the expansive KE jet provides a significant source of heat and moisture for the North Pacific midlatitude atmospheric storm tracks (Nakamura et al., 2004). By modifying the path and intensity of the wintertime overlying storm tracks, changes in the dynamic state of KE can alter not only the stability and pressure gradient within the local atmospheric boundary layer, but also the basin-scale wind stress pattern (Frankignoul and Sennéchael, 2007; Kwon et al., 2010). Specifically, a dynamically stable (unstable) KE tends to generate a positive (negative) wind stress curl in the eastern North Pacific basin, resulting in negative (positive) local SSH anomalies through Ekman divergence (convergence). This impact on wind stress induces a delayed negative feedback with a preferred period of about 10 years and is likely the cause for the enhanced decadal variance observed in the midlatitude North Pacific (Qiu et al., 2007b).

6. South Pacific

6.1. Upstream EAC

Mirroring the NEC bifurcation off the Philippine coast, the wind-driven, westward-flowing SEC splits upon reaching the Australian coast, feeding into the northward-flowing North Queensland Current and southward-flowing EAC (Ridgway and Dunn, 2003; see Figure 13.12b). Unlike its counterpart in the Northern Hemisphere, however, the SEC in the western South Pacific is heavily affected by complex topography. The presence of the island ridges of Fiji (near 18°S and 178°E), Vanuatu (near 15°S and 167°E), and New Caledonia (near 22°S and 165°E) fractures the SEC, channeling it into localized zonal jets known as the North and South Fiji Jets, the North and South Caledonian Jets, and the North Vanuatu Jet (Webb, 2000; Stanton et al., 2001; Gourdeau et al., 2008; Qiu et al., 2009). In addition, the existence of the shallow Queensland Plateau just south of the SEC bifurcation near 18°S causes the EAC to begin as a doubled boundary jet system straddling the Queensland Plateau.

Constrained by the basin-scale surface wind forcing, the transport of the SEC entering the Coral Sea between New Caledonia and the Solomon Islands (near 9°S and 160°E) is about 22 Sv. This SEC volume transport has a seasonal maximum in October–December and a minimum in April–June (Holbrook and Bindoff, 1999; Kessler and Gourdeau, 2007). Concurrent with its seasonal transport increase, the SEC bifurcation tends to shift equatorward in October–December, and is accompanied by a summer transport increase in EAC along the eastern coast of Australia. The amplitude of seasonal change of the EAC transport has been estimated at 4–6 Sv (Ridgway and Godfrey, 1997; Roemmich et al., 2005; Kessler and Gourdeau, 2007).

Compared to the interior Sverdrup transport of ~35 Sv along 30°S (Risien and Chelton, 2008), the observed poleward transport of the EAC is about 20–22 Sv (Ridgway and Godfrey, 1994; Mata et al., 2000). This discrepancy is largely due to the presence of an open western boundary in the equatorial Pacific, through which part of the SEC inflow is lost to the Indian Ocean via the Indonesian Throughflow, which is shown schematically northwest of Australia in Figure 1.6 (Godfrey, 1989).

6.2 East Australian Current

After the SEC’s bifurcation near 18°S, the poleward-flowing EAC evolves into a

narrow, swift boundary jet with strong vertical shear over the upper 1000 m. The EAC has short-term transport variations with a dominant timescale of 90–180 days (Mata et al., 2000; Bowen et al., 2005), likely caused by intrinsic nonlinear variability of the EAC (Bowen et al., 2005; Mata et al., 2006) or forced by eddy signals propagating into the EAC (Nilsson and Cresswell, 1981; Cresswell and Legeckis, 1986). Similar to the subtropical North Pacific, a high EKE band exists at latitudes 20–30°S in the western subtropical South Pacific (Figure 13.1). Dynamically, this high EKE band is caused by baroclinic instability of the surface, eastward-flowing Subtropical Countercurrent, and the underlying, westward-flowing SEC (Qiu and Chen, 2004).

The main flow of the EAC detaches from the Australian coast at 30–34°S and crosses the northern Tasman Sea. Like the Kuroshio in the Northern Hemisphere, the latitude of the EAC separation is located equatorward of the zero Sverdrup transport stream-function line in the South Pacific (along about 50°S; Risien and Chelton, 2008). The presence of New Zealand and the inertial nature of the EAC jet have been found to be responsible for this equatorward separation latitude of the EAC (Tillburg et al., 2001). Offshore, it separates into an eastward branch, known as the Tasman Front, and a northeastward branch that connects to the eastward-flowing Subtropical Countercurrent in the 20–30°S band. The path of the Tasman Front is influenced by the meridionally aligned Lord Howe Rise (along about 162°E) and Norfolk Ridge (along about 168°E), which it must negotiate. Over the Lord Howe Rise, the isotherms of the Tasman Front tend to detour southward before turning northward to wrap around the southern edge of the Norfolk Ridge and into the Norfolk Basin (Uddstrom and Oien, 1999). Along its path, the Tasman Front is highly variable and is often accompanied by wave-like disturbances that propagate westward against the direction of the background mean flow (Nilsson and Cresswell, 1981). After impinging upon the Australian coast, many of these disturbances develop into isolated cyclonic eddies, migrating poleward into the southern Tasman Sea. The cyclonic eddy detachment has a frequency of about three eddies per year.

After reaching the northern tip of New Zealand and joined by flows feeding in from the east, a portion of the Tasman Front turns southeastward, forming the East Auckland Current (EAUC) along the northeast coastline of the North Island of New Zealand. The southeastward transport of the EAUC is highly variable, with a mean value of about 9 Sv (Stanton, 2001; Stanton and Sutton, 2003). The EAUC is

renamed the East Cape Current after it flows around East Cape, the easternmost point of the North Island. Three topographically constrained, quasi-permanent, cyclonic eddies, known as the North Cape Eddy, the East Cape Eddy, and the Wairarapa Eddy, are observed along the EAUC and East Cape Current paths (Roemmich and Sutton, 1998). The subtropical-origin East Cape Current continues southward along the east coast of New Zealand until it turns eastward near 43°S to rejoin the interior Sverdrup circulation (Sutton, 2001), merging with the Southland Current to become the eastward-traveling South Pacific Current.

6.3. EAC Extension

While the main portion of the EAC separates from the Australian coast near 34°S, the remainder continues southward along the Australian coast to as far south as Tasmania and is known as the EAC Extension. *In situ* observations at the Maria Island coast station off the east coast of Tasmania reveal that both the temperature and salinity have increased steadily over the past 60 years, consistent with a southward expansion of the EAC Extension (Ridgway, 2007; Hill et al., 2008; see Figure 13.15a and b). Given temperature and salinity trends of 2.28 °C century^{-1} and 0.34 psu century^{-1}, observed at the Maria Island station, the EAC Extension is estimated to have expanded southward by about 350 km from 1944 to 2002. Over the same period, an increase in the net volume transport through the Tasman Sea is estimated at ~10 Sv (Figure 13.15d).

The poleward expansion of the EAC Extension occurs at the expense of the Tasman Front. In other words, the strengths of the EAC Extension and the Tasman Front are anticorrelated (Hill et al., 2011). Concurrent with the multidecadal poleward expansion of the EAC Extension into the southern Tasman Sea, a significant thermocline cooling has been detected in the northern EAC region from 1975 to 1990, reflecting the weakening of the upstream EAC (Ridgway and Godfrey, 1996).

The long-term intensification and southward expansion of the EAC Extension are caused by changes in the basin-scale surface wind field. Specifically, the strengthening and southward migration of the Southern Hemisphere westerlies enhance and expand the downward Ekman pumping in the subtropical South Pacific north of 50°S. These changes induce a spin-up and southward expansion of both the interior subtropical gyre and the EAC Extension, with the latter having a delay of adjustment of several years (Bowen et al., 2006; Qiu and Chen, 2006; Roemmich et

al., 2007; Hill et al., 2010; see Figure 13.15).

Note that rather than a confined change in the South Pacific, spin-up of the wind-driven subtropical gyre also occurs in the South Atlantic and Indian Oceans and is connected to the upward trend in the Southern Annular Mode signals of the Southern Hemisphere atmospheric circulation (Cai, 2006; Roemmich, 2007). On the western side of the Tasman Sea, some of the EAC Extension turns west south of Tasmania, and connects to the southern Indian Ocean subtropical circulation, forming the so-called Southern Hemisphere Supergyre (Speich et al., 2002; Ridgway and Dunn, 2007). This inter-ocean exchange is known as Tasman leakage. As the wind-driven South Pacific subtropical gyre intensifies and shifts southward, the "outflow" from the South Pacific to southern Indian Ocean likely intensifies. It is important for future studies to clarify how this outflow intensification can modify the global overturning circulation.

7. Concluding remarks

7.1. Separation from the western boundary

The latitude of separation of WBCs from their continental boundaries has an important impact on ocean circulation, air–sea fluxes, and even climate. Separation dynamics are subtle and this chapter has shown that different controls dominate the latitude of separation of each WBC. However, the latitude of separation is *always* lower than that inferred from linear wind-driven circulation theory.

In the North Atlantic, the separation latitude of the Gulf Stream is fairly stable, and interaction with the DWBC below the Gulf Stream and/or the NRG located north of the GSE seems to play an important role. In the South Atlantic, the separation latitude of the Brazil Current is less stable, probably because it collides with the fairly strong, northward-flowing Malvinas Current well before reaching the latitude of zero wind stress curl. It separates from the boundary with the Malvinas Current, as the Brazil–Malvinas Confluence.

In the Indian Ocean, the African continent disappears before the Agulhas Current reaches the latitude of zero wind stress curl. This fact results in leakage of Indian Ocean water into the South Atlantic, and retroflection of the Agulhas Current eastward to rejoin the Indian Ocean subtropical gyre. Theory suggests that the positions of separation and retroflection are linked and affect leakage.

In the North Pacific, the separation latitude of the Kuroshio is likely governed by the combined effects of the coastal geometry of Japan and the inertial nature of the Kuroshio and KE jet. In the South Pacific, the separation latitude of the EAC is quite variable because of the presence of New Zealand offshore and the inertial nature of the EAC jet. There is leakage of South Pacific water into the Indian Ocean as the EAC Extension turns west south of Tasmania.

7.2. Northern and Southern Hemispheres

The difference in land mass distribution between the Northern and Southern Hemispheres leads to fundamental differences among WBCs and the circulations they feed into. The Agulhas Current and EAC leak waters into the Atlantic and Indian Oceans, respectively, because they run out of western boundary well before the latitude of zero wind stress curl. This creates a Southern Hemisphere "super-gyre," which connects the subtropical gyres of the South Pacific, Indian, and South Atlantic Oceans. The Southern Hemisphere WBCs interact strongly with the Antarctic Circumpolar Current, especially in the Indian and Atlantic sectors, where heat is transported toward the pole via eddies associated with the WBC extensions. Heat loss over WBC extensions of the Northern Hemisphere tends to be stronger than over those of the Southern Hemisphere, because adjacent larger continental land masses on the west provide colder, dryer air masses over them.

The most conspicuous difference between the Northern and Southern Hemispheres is that there are far fewer observations of WBCs in the Southern Hemisphere. This is particularly acute for the Brazil and Agulhas Currents, where long-term observations are needed.

7.3. Recent and future studies

In the Gulf Stream, research on mesoscale variability and pathway prediction has decreased over the past two decades. The latest emphasis is primarily on the role of the Gulf Stream in the MOC and climate, and its variability on seasonal and longer timescales. Little attention has been given to obtaining new *in situ* observations of the Brazil Current and its confluence with the Malvinas Current historically, with the most recent studies relying heavily on the analysis of remote sensing observations (e.g., Lumpkin and Garzoli, 2011).

Research into the Agulhas Current has accelerated over the last 3–4 years, with

several international observation and modeling programs. However, many observations are coming to an end, and an international group of scientists is cooperating to establish a sustained array in the near future. Biastoch et al. (2009) developed a realistic simulation of the Agulhas Current system using a high-resolution, regional nest in a global ocean model. Climate modelers are becoming more interested in Agulhas Current research after the very recent advent of coupled climate models with eddy-resolving ocean models. For the Somali Current, there is growing interest in utilizing autonomous observing platforms, including Argo floats, underwater gliders, and surface drifters, in order to overcome the piracy problem in that region.

For the Kuroshio south of Japan, the research pace has been somewhat slow after the WOCE program, partly because the prominent large meander was absent. The KE research is strong, with recent interest focused on the KE jet and its recirculation gyre dynamics, carrying out intensive observations using a large set of inverted echo sounders equipped with bottom pressure gauges and current-meters. The role of KE front on the midlatitude atmospheric circulation is also targeted by an international group of oceanographers and meteorologists. For the EAC, observations using current-meter moorings, subsurface gliders, and hydrography are being pursued as a part of sustained marine observing system.

For future studies, we suggest four topics to be prioritized: air–sea interaction, boundary separation, submesoscale dissipation, and interaction with the deep ocean. The large heat and carbon fluxes between ocean and atmosphere associated with WBCs and their extensions are important topics in climate science. A better understanding of transfer processes and air–sea coupling on multiple timescales is needed. The separation latitudes of WBCs, as well as subsequently the mean latitude of WBC extensions, have a significant impact on regional meteorology and climate variability. Research into the dynamics of separation has exposed more possible mechanisms, but not yet identified which processes are most important. Our understanding of the mesoscale eddy variability of WBCs has improved due to an accumulation of *in situ* and satellite observations, and eddy-resolving numerical models. However, the dissipation of mesoscale variability is largely via submesoscale processes, which are largely unobserved and unresolved in general circulation models. Those processes can be addressed soon by remote sensing with the advent of the Surface Water and Ocean Topography satellite mission, which will

measure SSH with a spatial resolution of less than 10 km. Finally, our description of the pathways of deep WBCs and our understanding of the interaction between upper- and deep-ocean WBCs are still evolving beyond the seminal contributions of Stommel and Arons (1960a,b).

Acknowledgments

We thank two anonymous reviewers and the editors (G. Siedler and J. Gould) for constructive and valuable comments, which have improved the manuscript considerably. Lynne Talley, Pierre-Yves Le Traon, Hiroshi Uchida, and Heather Furey helped us prepare the figures.

References

Al Saafani, M. A., Shenoi, S. S. C., Shankar, D., Aparna, M., Kurian, J., Durand, F., & Vinayachandran, P. N. (2007). Westward movement of eddies into the Gulf of Aden from the Arabian Sea. *Journal of Geophysical Research, 112*, C11004, doi:10.1029/2006JC004020.

Anderson, D. L. T., & Corry, R. A. (1985). Seasonal transport variations in the Florida Straits: A model study. *Journal of Physical Oceanography, 15*, 773–786.

Anderson, D. L. T., & Moore, D. W. (1979). Cross-equatorial inertial jets with special relevance to the very remote forcing of the Somali Current. *Deep-Sea Research, 26*, 1–22.

Andres, M., Park, J.-H., Wimbush, M., Zhu, X.-H., Chang, K.-I., & Ichikawa, H. (2008). Study of the Kuroshio/Ryukyu Current system based on satellite-altimeter and *in situ* measurements. *Journal of Oceanography, 64*, 937–950.

Arhan, M., Mercier, H., & Park, Y-H. (2003). On the deep water circulation of the eastern South Atlantic Ocean. *Deep-Sea Research I, 50*, 889–916.

Auer, S. J. (1987). Five-year climatological survey of the Gulf Stream System and its associated rings. *Journal of Geophysical Research, 92*, 11,709–11,726.

Baringer, M., & Larsen, J. (2001). Sixteen years of Florida Current transport at 27°N. *Geophysical Research Letters, 28*, 3179–3182.

Beal, L. M. (2009). A time series of Agulhas Undercurrent transport. *Journal of Physical Oceanography, 39*, 2436–2450.

Beal, L. M., & Bryden, H. L. (1999). The velocity and vorticity structure of the Agulhas Current at 32°S. *Journal of Geophysical Research, 104*, 5151–5176.

Beal, L. M., & Chereskin, T. K. (2003). The volume transport of the Somali Current during the 1995 southwest monsoon. *Deep-Sea Research II, 50*, 2077–2089.

Beal, L. M., Chereskin, T. K., Bryden, H. L., & Ffield, A. (2003). Variability of water properties, heat and salt fluxes in the Arabian Sea, between the onset and wane of the 1995 southwest monsoon. *Deep-Sea Research II, 50*, 2049–2075.

Beal, L. M., Chereskin, T. K., Lenn, Y. D. & Elipot, S. (2006). The sources and mixing characteristics of the Agulhas Current. *Journal of Physical Oceanography, 36*, 2060–2074.

Beal, L. M., de Ruijter, W. P. M., Biastoch, A., Zahn, R., & SCOR/WCRP/IAPSO Working Group 136 (2011). On the role of the Agulhas system in ocean circulation and climate, *Nature, 472*, 429–436, doi:10.1038/nature09983.

Beal, L. M., & Donohue, K. A. (2013). The Great Whirl: Observations of its seasonal development and interannual variability. *Journal of Geophysical Research*, *118*, 1–13, doi:10.1029/2012JC008198.

Beal, L. M., Hummon, J. M., Williams, E., Brown, O. B., Baringer, W., & Kearns, E. J. (2008). Five years of Florida Current structure and transport from the Royal Caribbean Cruise Ship *Explorer of the Seas*. *Journal of Geophysical Research, 113*, C06001, doi:10.1029/2007JC004154.

Behera, S. K., & Yamagata, T. (2001). Subtropical SST dipole events in the southern Indian Ocean. *Geophysical Research Letters, 28*, 327–330.

Biastoch, A., Böning, C. W., & Lutjeharms, J. R. E. (2008). Agulhas leakage dynamics affects decadal variability in Atlantic overturning circulation. *Nature, 456*, 489–492.

Biastoch, A., Böning, C. W., Schwarzkopf, F. U., & Lutjeharms, J. R. E. (2009). Increase in Agulhas leakage due to poleward shift of the Southern Hemisphere westerlies. *Nature, 462*, 495–498.

Boebel, O., Lutjeharms, J. R. E., Schmid, C., Zenk, W., Rossby, T., & Barron, C. N. (2003). The Cape Cauldron, a regime of turbulent inter-ocean exchange. *Deep-Sea Research II*, *50*, 57–86.

Bowen, M. M., Sutton, P. J. H., & Roemmich, D. (2006). Wind-driven and steric fluctuations of sea surface height in the southwest Pacific. *Geophysical Research Letters, 33*, L14617, doi:10.1029/2006GL026160.

Bowen, M. M., Wilkin, J. L., & Emery, W. J. (2005). Variability and forcing of the East Australian Current. *Journal of Geophysical Research, 110*, C03019, doi:10.1029/2004JC0222533.

Bower, A. S. (1991). A simple kinematic mechanism for mixing fluid parcels across a meandering jet. *Journal of Physical Oceanography, 21*, 173–180.

Bower, A. S., & Hogg, N. G. (1996). Structure of the Gulf Stream and its recirculations at 55°W. *Journal of Physical Oceanography, 26*, 1002–1022, doi:10.1175/1520–0485(1996)026<1002:SOTGSA>2.0.CO;2.

Bower, A. S., Le Cann, B., Rossby, H. T., Zenk, W., Gould, J., Speer, K., Richardson, P. L., Prater, M. D., & Zhang, H.-M. (2002). Directly measured mid-depth circulation in the northeastern North Atlantic Ocean. *Nature, 419*, 603–607.

Bower, A. S., & Lozier, M. S. (1994). A closer look at particle exchange in the Gulf Stream. *Journal of Physical Oceanography, 24*, 1399–1418.

Bower, A. S., & Rossby, T. (1989). Evidence of cross-frontal exchange processes in the Gulf Stream based on isopycnal RAFOS float data. *Journal of Physical Oceanography, 19*, 1177–1190.

Bower, A. S., Rossby, H. T., & Lillibridge, J. L. (1985). The Gulf Stream – Barrier or blender? *Journal of Physical Oceanography*, *15*, 24–32.

Brandt, P., Stramma, L., Schott, F., Fischer, J., Dengler, M., & Quadfasel, D. (2002). Annual Rossby waves in the Arabian Sea from TOPEX/Poseidon altimeter and in situ data. *Deep-Sea Research, 50*, 1197–1210.

Bryan, F. O., Hecht, M. W., & Smith, R. D. (2007). Resolution convergence and sensitivity studies with North Atlantic circulation models. Part I: The western boundary current system. *Ocean Modelling*, *16*, 141–159.

Bryden, H. L., Beal, L. M., & Duncan, L. M. (2005). Structure and transport of the Agulhas Current and its temporal variability. *Journal of Oceanography, 61*, 479–492.

Cai, W. (2006). Antarctic ozone depletion causes an intensification of the Southern Ocean super-gyre circulation. *Geophysical Research Letters, 33*, L03712, doi:10.1029/2005GL024911.

Cane, M. (1980). On the dynamics of equatorial currents, with application to the Indian Ocean. *Deep-Sea Research, 27A*, 525–544.

Carr, M.-E., & Rossby, H. T. (2000). Pathways of the North Atlantic Current from surface drifters and subsurface floats. *Journal of Geophysical Research*, *106*, 4405–4419.

Carton, J.A., Chepurin, G., Cao, X., & Giese, B. S. (2000). A Simple Ocean Data Assimilation analysis of the global upper ocean 1950–1995, Part 1: Methodology, *Journal of Physical Oceanography, 30*, 294–309.

Centurioni, L. R., Niiler, P. P., & Lee, D.-K. (2004). Observations of inflow of Philippine Sea water into the South China Sea through the Luzon Strait. *Journal of Physical Oceanography, 34*, 113–121.

Charney, J. G. (1955). The Gulf Stream as an inertial boundary layer. *Proceedings of the National Academy of Sciences of the U.S.A., 41*, 731–740.

Chassignet, E. P., & Garraffo, Z. D. (2001). Viscosity parameterization and the Gulf Stream separation. In *From Stirring to Mixing in a Stratified Ocean: Proceedings of the 12th 'Aha Huliko'a Hawaiian Winter Workshop, 2001,* (pp. 39–43), University of Hawaii at Manoa, Honolulu.

Chiessi, C. M. et al. (2008). South Atlantic interocean exchange as the trigger for the Bølling warm event. *Geology, 36,* 919–922.

The Climode Group (2009). The Climode Field Campaign: Observing the cycle of convection and restratification over the Gulf Stream. *Bulletin of the American Meteorological Society, 90,* 1337–1350.

Cox, M. D. (1979). A numerical study of Somali Current eddies. *Journal of Physical Oceanography, 9,* 311–326.

Cresswell, G. R., & Legeckis, R. (1986). Eddies off southeastern Australia. *Deep-Sea Research, 22,* 1527–1562.

Cronin, M., & Co-Authors (2010). Monitoring ocean–atmosphere interactions in western boundary current extensions. In J. Hall, D.E. Harrison & D. Stammer (Eds.), *Proceedings of OceanObs'09: Sustained Ocean Observations and Information for Society (Vol. 2),* Venice, Italy, 21–25 September 2009, ESA Publication WPP-306, doi:10.5270/OceanObs09.cwp.20.

Cronin, M. F., & Watts, D. R. (1996). Eddy–mean flow interaction in the Gulf Stream at 68°W. Part 1: Eddy energetics. *Journal of Physical Oceanography, 26,* 2107–2131.

Cushman-Roisin, B. (1993). Trajectories in Gulf Stream meanders. *Journal of Geophysical Research, 98,* 2543–2554.

Davis, R., & Zenk, W. (2001). Subsurface Lagrangian observations during WOCE. In G. Siedler, J. Church & J. Gould (Eds.), *Ocean Circulation and Climate* (pp. 123–139). *International Geophysics Series*, Vol. 77, Academy Press, New York.

Dencausse, G., Arhan, M., & Speich, S. (2010). Spatio-temporal characteristics of the Agulhas Current retroflection. *Deep-Sea Research I, 57,* 1392–1405.

Dengg, J., Beckmann, A., & Gerdes, R. (1996). The Gulf Stream separation problem. In W. Krauss (Ed.), *The warmwatersphere of the North Atlantic Ocean* (pp. 253–290). Gebruder Borntrager, Stuttgart.

de Ruijter, W. P. M. (1982). Asymptotic analysis of the Agulhas and Brazil Current systems. *Journal of Physical Oceanography, 12,* 361–373.

de Ruijter, W. P. M., Biastoch, A., Drijfhout, S. S., Lutjeharms, J. R. E., Matano, R. P., Pichevin, T., van Leeuwen, P. J., & Weijer, W. (1999). Indian–Atlantic inter-ocean exchange: Dynamics, estimation, and impact. *Journal of Geophysical Research, 104,* 20,885–20,910.

de Ruijter, W. P. M., van Aken, H. M., Beier, E. J., Lutjeharms, J. R. E., Matano, R. P., & Schouten, M. W. (2004). Eddies and dipoles around South Madagascar: Formation, pathways and large-scale impact. *Deep-Sea Research, 51,* 383–400.

Dibarboure, G., Pujol, M.-I., Briol, F., Le Traon, P. Y., Larnicol, G., Picot, N., Mertz, F., & Ablain, M. (2011). Jason-2 in DUACS: Updated system description, first tandem results and impact on processing and products. *Marine Geodesy, 34*, 214–241.

DiNezio, P. N., Gramer, L. J., Johns, W. E., Meinen, C. S., & Baringer, M. O. (2009). Observed interannual variability of the Florida Current: Wind forcing and the North Atlantic Oscillation. *Journal of Physical Oceanography, 39*, 721–736, doi:10.1175/2008JPO4001.1.

Donlon, C., & Coauthors (2007). The Global Ocean Data Assimilation Experiment High-resolution Sea Surface Temperature Pilot Project. *Bulletin of the American Meteorological Society, 88*, 1197–1213, doi:10.1175/BAMS-88-8-1197.

Donohue, K. A., & Toole, J. M. (2003). A near-synoptic survey of the southwest Indian Ocean. *Deep-Sea Research II, 50*, 1893–1931.

Duan, J., & Wiggins, S. (1996). Fluid exchange across a meandering jet with quasiperiodic variability. *Journal of Physical Oceanography*, *26*, 1176–1188.

Ducet, N., Le Traon, P. Y., & Reverdin, G. (2000). Global high-resolution mapping of ocean circulation from TOPEX/Poseidon and ERS-1 and -2. *Journal of Geophysical Research, 105*, 19,477–19,498.

Ducklow, H. W., Steinberg, D. K., & Buesseler, K. O. (2001). Upper ocean carbon export and the biological pump. *Oceanography, 14*, 50–58, http://dx.doi.org/10.5670/oceanog.2001.06

Düing, W., Molinari, R. L., & Swallow, J. C. (1980). Somali Current: Evolution of surface flow, *Science*, *209*, 588–590.

Evans, D. L., & Signorini, S. S. (1985). Vertical structure of the Brazil Current. *Nature*, *315*, 48–50.

Ezer, T., & Mellor, G. L. (1992). A numerical study of the variability and the separation of the Gulf Stream induced by surface atmospheric forcing and lateral boundary flows. *Journal of Physical Oceanography*, *22*, 660–682.

Feng, M., Mitsudera, H., & Yoshikawa, Y. (2000). Structure and variability of the Kuroshio Current in Tokara Strait. *Journal of Physical Oceanography, 30*, 2257–2276.

Ffield, A., Toole, J., & Wilson, D. (1997). Seasonal circulation in the south Indian Ocean. *Geophysical Research Letters*, *24*, 2773–2776.

Findlater, J. (1969). A major low-level air current near the Indian Ocean during the northern summer. *Quarterly Journal of the Royal Meteorological Society, 95*, 280–362.

Fine, R. A. (1993). Circulation of Antarctic Intermediate Water in the South Indian Ocean. *Deep Sea Research I, 40*, 2021–2042.

Fischer, J., & Schott, F. A. (2002). Labrador Sea Water tracked by profiling floats – From the boundary current into the open North Atlantic. *Journal of Physical Oceanography, 32*, 573–584.

Fischer, J., Schott, F., & Stramma, L. (1996). Current transports of the Great Whirl–Socotra Gyre system during summer monsoon, August 1993. *Journal of Geophysical Research, 101*, 3573–3687.

Fofonoff, N. P. (1981). The Gulf Stream system. In B. A. Warren & C. Wunsch (Eds.), *Evolution of Physical Oceanography* (pp. 112–139). MIT Press, Cambridge, Mass.

Frankignoul, C., de Coetlogon, G., Joyce, T., & Dong, S. (2001). Gulf Stream variability and ocean–atmosphere interactions. *Journal of Physical Oceanography, 31*, 3516–3529, doi:10.1175/1520-0485(2002)031<3516:GSVAOA>2.0.CO;2.

Frankignoul, C., & Sennéchael, N. (2007). Observed influence of North Pacific SST anomalies on the atmospheric circulation. *Journal of Climate, 20*, 592–606.

Fratantoni, D. (2001). North Atlantic surface circulation during the 1990's observed with satellite-tracked drifters. *Journal of Geophysical Research, 106*, 22,067–22,093, doi:10.1029/2000JC000730.

Fratantoni, D. M., Bower, A. S., Johns, W. E., & Peters, H. (2006). Somali Current rings in the eastern Gulf of Aden. *Journal of Geophysical Research, 111*, C09039, doi:10.1029/2005JC003338.

Garfield, N. (1990). *The Brazil Current at subtropical latitudes*. PhD Thesis, University of Rhode Island, 122 pp.

Garzoli, S. L. (1993). Geostrophic velocity and transport variability in the Brazil–Malvinas Confluence. *Deep-Sea Research, 40*, 1379–1403.

Garzoli, S. L., & Giulivi, C. (1994). What forces the variability of the southwestern Atlantic boundary currents? *Deep-Sea Research I, 41*, 1527–1550.

Garzoli, S. L., Goni, G. J., Mariano, A., & Olson, D. (1997). Monitoring the upper southeastern Atlantic transport using altimeter data. *Journal of Marine Research, 55*, 453–481.

Garzoli, S. L., & Matano, R. (2011). The South Atlantic and the Atlantic Meridional

Overturning Circulation. *Deep-Sea Research II*, *58*, 1837–1847.

Gilson, J., & Roemmich, D. (2002). Mean and temporal variability in the Kuroshio geostrophic transport south of Taiwan (1993–2001). *Journal of Oceanography, 58*, 183–195.

Gimeno, L., Drumond, A., Nieto, R., Trigo, R. M., & Stohl, A. (2010). On the origin of continental precipitation. *Geophysical Research Letters*, *37*, L13804, doi:10.1029/2010GL043712.

Godfrey, J. S. (1989). A Sverdrup model of the depth-integrated flow for the world ocean allowing for island circulations. *Geophysical and Astrophysical Fluid Dynamics, 45*, 89–112.

Goni, G. J., Garzoli, S. L., Roubicek, A. J., Olson, D. B., & Brown, O. B. (1997). Agulhas ring dynamics from TOPEX/POSEIDON satellite altimeter data. *Journal of Marine Research*, *55*, 861–883.

Goni, G. J., & Wainer, I. (2001). Investigation of the Brazil Current front variability from altimeter data. *Journal of Geophysical Research, 106*, 31,117–31,128, doi:10.1029/2000JC000396.

Gordon, A. L. (1989). Brazil–Malvinas Confluence – 1984. *Deep-Sea Research*, *36*, 359–384.

Gordon, A. L., & Greengrove, C. L. (1986). Geostrophic circulation of the Brazil–Falkland confluence. *Deep-Sea Research, 33*, 573–585.

Gordon, A. L., Weiss, R. F., Smethie, W. M., & Warner, M. J. (1992). Thermocline and Intermediate Water communication between the South Atlantic and Indian Oceans. *Journal of Geophysical Research, 97*, 7223–7240.

Gourdeau, L., Kessler, W. S., Davis, R. E., Sherman, J., Maes, C., & Kestenare, E. (2008). Zonal jets entering the Coral Sea. *Journal of Physical Oceanography, 38*, 715–725.

Grundlingh, M. (1979). Observation of a large meander in the Agulhas Current. *Journal of Geophysical Research, 84*, 3776–3778.

Grundlingh, M. (1983). On the course of the Agulhas Current. *South African Geographical Journal, 65*, 49–57.

Halkin, D., & Rossby, T. (1985). The structure and transport of the Gulf Stream at 73°W. *Journal of Physical Oceanography, 15*, 1439–1452, doi:10.1175/1520-0485(1985)015<1439:TSATOT>2.0.CO;2.

Halpern, D., & Woiceshyn, P. M. (1999). Onset of the Somali Jet in the Arabian Sea during June 1997. *Journal of Geophysical Research, 104*, 18,041–18,046.

Hanawa, K., & Talley, L. D. (2001). Mode waters. In G. Siedler, J. Church & J. Gould (Eds.), *Ocean Circulation and Climate* (pp. 373–386). *International Geophysics Series*, Vol. 77, Academy Press, New York.

Hastenrath, S., & Greischar, L. (1991). The Monsoonal current regimes of the tropical Indian Ocean: Observed surface flow fields and their geostrophic and wind-driven components. *Journal of Geophysical Research*, *96*, 12,619–12,633.

Hecht, M. W., & Smith, R. D. (2008). Towards a physical understanding of the North Atlantic: A review of model studies in an eddying regime. In M. W. Hecht & H. Hasumi (Eds.), *Ocean Modeling in an Eddying Regime* (pp. 213–239). *Geophysical Monograph Series*, vol. 177, American Geophysical Union, Washington, D. C., doi:10.1029/177GM15.

Hellerman, S., & Rosenstein, M. (1983). Normal monthly wind stress over the world ocean with error estimate. *Journal of Physical Oceanography*, *13*, 1093–1104.

Hill, K .L., Rintoul, S. R., Coleman, R., & Ridgway, K. R. (2008). Wind forced low frequency variability of the East Australia Current. *Geophysical Research Letters, 35*, L08602, doi:10.1029/2007GL032912.

Hill, K. L., Rintoul, S. R., Oke, P. R., & Ridgway, K. R. (2010). Rapid response of the East Australian Current to remote wind forcing: The role of barotropic–baroclinic interactions. *Journal of Marine Research, 68*, 413–431.

Hill, K. L., Rintoul, S. R., Ridgway, K. R., & Oke, P. R. (2011). Decadal changes in the South Pacific western boundary current system revealed in observations and ocean state estimates. *Journal of Geophysical Research*, *116*, C01009, doi:10.1029/2009JC005926.

Hogg, N. G. (1992). On the transport of the Gulf Stream between Cape Hatteras and the Grand Banks. *Deep-Sea Research, 39*, 1231–1246, doi:10.1016/0198-0149(92)90066-3.

Hogg, N. G., & Johns, W. E. (1995). Western boundary currents. *Review of Geophysics, 33*, 1311–1334, doi:10.1029/95RG00491.

Holbrook, N. J., & Bindoff, N. L. (1999). Seasonal temperature variability in the upper southwest Pacific Ocean. *Journal of Physical Oceanography*, *29*, 366–381.

Hoskins, B. J., & Hodges, K. I. (2002). New perspectives on the Northern Hemisphere winter storm tracks. *Journal of the Atmospheric Sciences*, *59*, 1041–1061.

Huang, R. X. (2010). *Ocean circulation: Wind-driven and thermohaline processes*. Cambridge University Press, Cambridge, 791 pp.

Hurlburt, H. E., Wallcraft, A. J., Schmitz Jr., W. J., Hogan, P. J., & Metzger, E. J. (1996). Dynamics of the Kuroshio/Oyashio current system using eddy-resolving models of the North Pacific Ocean. *Journal of Geophysical Research, 101*, 941–976.

Hurrell, J. (1995). Decadal trends in the North Atlantic Oscillation: Regional temperatures and precipitation. *Science, 269*, 676–679.

Ichikawa, H., & Beardsley, R. C. (1993). Temporal and spatial variability of volume transport of the Kuroshio in the East China Sea. *Deep-Sea Research, 40*, 583–605.

Ichikawa, H., Nakamura, H., Nishina, A., & Higashi, M. (2004). Variability of north-eastward current southeast of northern Ryukyu Islands. *Journal of Oceanography, 60*, 351–363.

Imawaki, S., Uchida, H., Ichikawa, H., Fukasawa, M., Umatani, S., & the ASUKA Group (2001). Satellite altimeter monitoring the Kuroshio transport south of Japan. *Geophysical Research Letters, 28*, 17–20.

Isobe, A., & Imawaki, S. (2002). Annual variation of the Kuroshio transport in a two-layer numerical model with a ridge. *Journal of Physical Oceanography, 32*, 994–1009.

Izumo, T., de Boyer Montégut, C., Luo, J-J., Behera, S. K., Masson, S., & Yamagata, T. (2008). The role of the western Arabian Sea upwelling in Indian monsoon rainfall variability. *Journal of Climate, 21*, 5603–5623.

James, C., Wimbush, M., & Ichikawa, H. (1999). Kuroshio meanders in the East China Sea. *Journal of Physical Oceanography, 29*, 259–272.

Jayne, S., Hogg, N., Waterman, S., Rainville, L., Donahue, K., Watts, D., Tracey, K., McClean, J., Maltrud, M., Qiu, B., Chen, S., & Hacker, P. (2009). The Kuroshio Extension and its recirculation gyres. *Deep-Sea Research, 56*, 2088–2099.

Jensen, T. G. (1991). Modeling the seasonal undercurrents in the Somali Current system. *Journal of Geophysical Research, 96,* 22,151–22,167.

Johns, W. E., Lee, T. N., Beardsley, R. C., Candela, J., Limeburner, R., & Castro, B. (1998). Annual cycle and variability of the North Brazil Current. *Journal of Physical Oceanography, 28*, 103–128.

Johns, W. E., Lee, T. N., Zhang, D., Zantopp, R., Liu, C.-T., & Yang, Y. (2001). The Kuroshio east of Taiwan: Moored transport observations from the WOCE PCM-1 array. *Journal of Physical Oceanography, 31*, 1031–1053.

Johns, W. E., Shay, T. J., Bane, J. M., & Watts, D. R. (1995). Gulf Stream structure, transport, and recirculation near 68°W. *Journal of Geophysical Research, 100*,

817–838, doi:10.1029/94JC02497.

Joyce, T. M., Deser, C., & Spall, M. A. (2000). The relation between decadal variability of subtropical mode water and the North Atlantic Oscillation. *Journal of Climate*, *13*, 2550–2569.

Joyce, T., Kwon, Y.-O., & Yu, L. (2009). On the relationship between synoptic wintertime atmospheric variability and path shifts in the Gulf Stream and the Kuroshio Extension. *Journal of Climate*, *22*, 3177–3192.

Jury, M., & Walker, N. (1988). Marine boundary layer modification across the edge of the Agulhas Current. *Journal of Geophysical Research, 93*, 647–654.

Kashino, Y., Espana, N., Syamsudin, F., Richards, K. J., Jensen, T., Dutrieux, P., & Ishida, A. (2009). Observations of the North Equatorial Current, Mindanao Current, and the Kuroshio Current system during the 2006/07 El Niño and 2007/08 La Niña. *Journal of Oceanography, 65*, 325–333.

Kawabe, M. (1988). Variability of Kuroshio velocity assessed from the sea level difference between Naze and Nishinoomote. *Journal of the Oceanographical Society of Japan, 44*, 293–304.

Kawabe, M. (1995). Variations of current path, velocity, and volume transport of the Kuroshio in relation with the large meander. *Journal of Physical Oceanography, 25*, 3103–3117.

Kearns, E. J., & Rossby, H. T. (1998). Historical position of the North Atlantic Current. *Journal of Geophysical Research, 103*, 15,509–15,524.

Kelly, K. A., Singh, S., & Huang, R. X. (1999). Seasonal variations of sea surface height in the Gulf Stream region. *Journal of Physical Oceanography, 29,* 313–327.

Kelly, K. A., Small, R. J., Samelson, R. M., Qiu, B., Joyce, T. M., Kwon, Y., & Cronin, M. F. (2010). Western boundary currents and frontal air-sea interaction: Gulf Stream and Kuroshio Extension. *Journal of Climate, 23*, 5644–5667, doi:10.1175/2010JCLI3346.1.

Kessler, W. S., & Gourdeau, L. (2007). The annual cycle of circulation of the southwest subtropical Pacific, analyzed in an ocean GCM. *Journal of Physical Oceanography, 37,* 1610–1627.

Kim, Y., Qu, T., Jensen, T., Miyama, T., Mitsudera, H., Kang, H., & Ishida, A. (2004). Seasonal and interannual variations of the North Equatorial Current bifurcation in a high-resolution OGCM. *Journal of Geophysical Research, 109*, C03040, doi:10.1029/2003JC002013.

Knorr, G., & Lohmann, G. (2003). Southern Ocean origin for the resumption of Atlantic thermohaline circulation during deglaciation. *Nature, 424*, 532–536.

Krauss, W., Fahrbach, E., Aitsam, A., Elken, J., & Koske, P. (1987). The North Atlantic Current and its associated eddy field southeast of Flemish Cap. *Deep-Sea Research, 34*, 1163–1185.

Kwon, Y., Alexander, M. A., Bond, N. A., Frankignoul, C., Nakamura, H., Qiu, B., & Thompson, L. (2010). Role of the Gulf Stream and Kuroshio–Oyashio systems in large-scale atmosphere–ocean interaction: A review. *Journal of Climate, 23*, 3249–3281, doi:10.1175/2010JCLI3343.1.

Larsen, J. C. (1992). Transport and heat flux of the Florida Current at 27°N derived from cross-stream voltages and profiling data: Theory and observation. *Philosophical Transactions of the Royal Society of London, 338*, 169–236.

Larsen, J. C., & Sanford, T. B. (1985). Florida Current volume transports from voltage measurements. *Science, 227*, 302–304.

Lazier, J. R. N. (1994). Observations in the Northwest Corner of the North Atlantic Current. *Journal of Physical Oceanography, 24*, 1449–1463.

Leaman, K. D., Molinari, R. L., & Vertes, P. S. (1987). Structure and variability of the Florida Current at 27°N: April 1982–July 1984. *Journal of Physical Oceanography, 17*, 565–583.

Lee, T., & Cornillon, P. (1995). Temporal variation of meandering intensity and domain-wide lateral oscillations of the Gulf Stream. *Journal of Geophysical Research, 100*, 13,603–13,613.

Lee, T., & Cornillon, P. (1996a). Propagation of Gulf Stream meanders between 74° and 70°W. *Journal of Physical Oceanography, 26*, 205–224.

Lee, T., & Cornillon, P. (1996b). Propagation and growth of Gulf Stream meanders between 75° and 45°W. *Journal of Physical Oceanography, 26*, 225–241.

Lee, T. N., Johns, W. E., Liu, C.-T., Zhang, D., Zantopp, R., & Yang, Y. (2001). Mean transport and seasonal cycle of the Kuroshio east of Taiwan with comparison to the Florida Current. *Journal of Geophysical Research, 106*, 22,143–22,158.

Lee, T. N., Schott, F. A., & Zantopp, R. J. (1985). Florida Current: Low-frequency variability as observed with moored current meters during April 1982 to June 1983. *Science, 227*, 298–302.

Lee-Thorp, A. M., Rouault, M., & Lutjeharms, J. R. E. (1998). Cumulus cloud formation above the Agulhas Current. *South African Journal of Science, 94*, 351–354.

Leetmaa, A, Quadfasel, D. R., & Wilson, D. (1982). Development of the flow field during the onset of the Somali Current, 1979. *Journal of Physical Oceanography, 12*, 1325–1342.

Lie, H.-J., Cho, C.-H., Lee, J.-H., Niiler, P. P., & Hu, J.-H. (1998). Separation of the Kuroshio water and its penetration onto the continental shelf west of Kyushu. *Journal of Geophysical Research, 103*, 2963–2976.

Lozier, M. S., Bold, T. J., & Bower, A. S. (1996). The influence of propagating waves on cross-stream excursions. *Journal of Physical Oceanography, 26*, 1915–1923.

Lozier, M. S., Pratt, L. J., Rogerson, A. M., & Miller, P. D. (1997). Exchange geometry revealed by float trajectories in the Gulf Stream. *Journal of Physical Oceanography*, *27*, 2327–2341.

Lumpkin, R., & Garraffo, Z. (2005). Evaluating the decomposition of tropical Atlantic drifter observations. *Journal of Atmospheric and Oceanic Technology, 22*, 1403–1415.

Lumpkin, R., & Garzoli, S. (2011). Interannual to decadal changes in the western South Atlantic's surface circulation. *Journal of Geophysical Research*, *116*, C01014, doi:10.1029/2010JC006285.

Luther, M. E. (1999). Interannual variability in the Somali Current 1954–1976. *Nonlinear Analysis, 35*, 59–83.

Lutjeharms, J. R. E. (2006). *The Agulhas Current*, Springer, Berlin, 330 pp.

Lutjeharms, J. R. E., & Ansorge, I. J. (2001). The Agulhas Return Current. *Journal of Marine Systems, 30*, 115–138.

Lutjeharms, J. R. E., & Roberts, H. R. (1988). The Natal Pulse: An extreme transient on the Agulhas Current. *Journal of Geophysical Research*, *93*, 631–645.

Lutjeharms, J. R. E., & van Ballegooyen, R. C. (1988). The retroflection of the Agulhas Current. *Journal of Physical Oceanography, 18*, 1570–1583.

Mann, C. R. (1967). The termination of the Gulf Stream and the beginning of North Atlantic Current. *Deep-Sea Research, 14*, 337–359, doi:10.1016/0011-7471(67)90077-0.

Mata, M. M., Tomczak, M., Wijffels, S., & Church, J. A. (2000). East Australian Current volume transports at 30°S: Estimates from the World Ocean Circulation Experiment hydrographic sections PR11/P6 and the PCM3 current meter array. *Journal of Geophysical Research, 105*, 28,509–28,526.

Mata, M. M., Wijffels, S. E., Church, J. A., & Tomczak, M. (2006). Eddy shedding and energy conversions in the East Australian Current. *Journal of Geophysical*

Research, 111, C09034, doi:10.1029/2006JC003592.

Matano, R. P. (1993). On the separation of the Brazil Current from the coast. *Journal of Physical Oceanography*, *23*, 79–90.

Matano, R. P., Beier, E. J., Strub, P. T., & Tokmakian, R. (2002). Large-scale forcing of the Agulhas variability: The seasonal cycle. *Journal of Physical Oceanography*, *32*, 1228–1241.

McCartney, M., & Zemba, J. (1988). Thermocline, intermediate and deep circulation in the southwestern South Atlantic. Abstract in: *SAARI Meeting Report, May 24–26, 1988*, Lamont-Doherty Geological Observatory of Columbia University, Palisades, New York, 28–29.

McCreary, J. P., & Kundu, P. K. (1988). A numerical investigation of the Somali Current during the southwest monsoon. *Journal of Marine Research*, *46*, 25–58.

Meinen, C. S., Baringer, M. O., & Garcia, R. F. (2010). Florida Current transport variability: An analysis of annual and longer-period signals. *Deep-Sea Research I, 57*, 835–846, doi:10.1016/j.dsr.2010.04.001.

Meinen, C. S., & Watts, D. R. (2000). Vertical structure and transport on a transect across the North Atlantic Current near 42°N: Time series and mean. *Journal of Geophysical Research, 105*, 21,869–21,891.

Minobe, S., Kuwano-Yoshida, A., Komori, N., Xie, S., & Small, R. J. (2008). Influence of the Gulf Stream on the troposphere. *Nature, 452*, 206–209.

Mizuno, K., & White, W. B. (1983). Annual and interannual variability in the Kuroshio Current system. *Journal of Physical Oceanography, 13*, 1847–1867.

Molinari, R. L., Wilson, W. D., & Leaman, K. (1985). Volume and heat transports of the Florida Current: April 1982 through August 1983. *Science, 227*, 295–297.

Munk, W. H. (1950). On the wind-driven ocean circulation. *Journal of Meteorology*, *7*, 79–93.

Munk, W. H., Gross, G. W., & Carrier, G. F. (1950). Note on the dynamics of the Gulf Stream. *Journal of Marine Research, 9*, 218–238.

Nakamura, H., Nishina, A., & Minobe, S. (2012). Response of storm tracks to bimodal Kuroshio path states south of Japan. *Journal of Climate*, 25, 7772–7779. doi:10.1175/JCLI-D-12-00326.1.

Nakamura, H., Sampe, T., Tanimoto, Y., & Shimpo, A. (2004). Observed associations among storm tracks, jet streams, and midlatitude oceanic fronts. In C. Wang, S.-P. Xie & J. A. Carton (Eds.), *Earth's Climate: The Ocean-Atmosphere Interaction* (pp. 329–346). *Geophysical Monograph Series,* vol. 147, American Geophysical Union, Washington, D. C.

Nakamura, H., & Shimpo, A. (2004). Seasonal variations in the Southern Hemisphere storm tracks and jet streams as revealed in reanalysis datasets. *Journal of Climate*, *17*, 1828–1844.

Nauw, J. J., van Aken, H. M., Webb, A., Lutjeharms, J. R. E., & de Ruijter, W. P. M. (2008). Observations of the southern East Madagascar Current and undercurrent and countercurrent system. *Journal of Geophysical Research, 113*, C08006, doi:10.1029/2007JC004639.

Niiler, P. P., & Richardson, W. S. (1973). Seasonal variability in the Florida Current. *Journal of Marine Research*, *21*, 144–167.

Nilsson, C. S., & Cresswell, G. R. (1981). The formation and evolution of East Australian Current warm-core eddies. *Progress in Oceanography, 9*, 133–183.

Nitani, H. (1972). Beginning of the Kuroshio. In H. Stommel & K. Yoshida (Eds.), *Kuroshio: Its Physical Aspects* (pp. 129–163). University of Tokyo Press, Tokyo.

Nof, D., & Pichevin, T. (1996). The retroflection paradox. *Journal of Physical Oceanography*, *26*, 2344–2358.

Oka, E. (2009). Seasonal and interannual variation of North Pacific Subtropical Mode Water in 2003–2006. *Journal of Oceanography, 65*, 151–164.

Oka, E., Suga, T., Sukigara, C., Toyama, K., Shimada, K., & Yoshida, J. (2011). "Eddy-resolving" observation of the North Pacific Subtropical Mode Water. *Journal of Physical Oceanography, 41*, 666–681.

Olson, D., Podesta, G., Evans, R., & Brown, O. (1988). Temporal variations in the separation of the Brazil and Malvinas Currents. *Deep-Sea Research*, *35*, 1971–1990.

O'Neill, L. W., Chelton, D. B., Esbensen, S. K., & Wentz, F. J. (2005). High-resolution satellite measurements of the atmospheric boundary layer response to SST variations along the Agulhas Return Current. *Journal of Climate, 18*, 2706–2723.

Orvik, K. A., & Niiler, P. (2002). Major pathways of Atlantic water in the northern North Atlantic and Nordic Seas toward Arctic. *Geophysical Research Letters*, *29*, 1896, doi:10.1029/2002GL015002.

Ou, H. W., & de Ruijter, W. P. M. (1986). Separation of an internal boundary current from a curved coast line. *Journal of Physical Oceanography*, *16*, 280–289.

Owens, W. B. (1991). A statistical description of the mean circulation and eddy variability in the northwestern North Atlantic using SOFAR floats. *Progress in*

Oceanography, 28, 257–303.

Pedlosky, J. (1996). *Ocean circulation theory*, Springer-Verlag, Berlin, 453 pp.

Peeters, F. J. C. et al. (2004). Vigorous exchange between the Indian and Atlantic oceans at the end of the past five glacial periods. *Nature, 430,* 661–665.

Peña-Molino, B., & Joyce, T. M. (2008). Variability in the slope water and its relation to the Gulf Stream path. *Geophysical Research Letters*, *35*, L03606, doi:10:10.1029/2007GL032183.

Penven, P., Lutjeharms, J. R. E., & Florenchie, P. (2006). Madagascar: A pacemaker for the Agulhas Current system? *Geophysical Research Letters*, *33*, L17609, doi:10.1029/2006GL026854.

Pérez-Brunius, H., Rossby, T., & Watts, D. R. (2004a). A method for obtaining the mean transports of ocean currents by combining isopycnal float data with historical hydrography. *Journal of Atmospheric and Oceanic Technology*, *21*, 298–316.

Pérez-Brunius, H., Rossby, T., & Watts, D. R. (2004b). Absolute transports of mass and temperature for the North Atlantic Current – Subpolar front system. *Journal of Physical Oceanography*, *34*, 1870–1883.

Peterson, R. G. (1990). On the volume transport in the southwestern South Atlantic Ocean. Abstract in: *Eos, Transactions, American Geophysical Union, 71*, 542.

Peterson, R. G., & Stramma, L. (1991). Upper-level circulation in the South Atlantic Ocean. *Progress in Oceanography*, *26*, 1–73.

Pichevin, T., Nof, D., & Lutjeharms, J. R. E. (1999). Why are there Agulhas rings? *Journal of Physical Oceanography*, *29*, 693–707.

Pratt, L. J., Lozier, M. S., & Beliakova, N. (1995). Parcel trajectories in quasigeostrophic jets: Neutral modes. *Journal of Physical Oceanography, 25*, 1451–1466.

Qiu, B. (1999). Seasonal eddy field modulation of the North Pacific Subtropical Countercurrent: TOPEX/POSEIDON observations and theory. *Journal of Physical Oceanography, 29*, 2471–2486.

Qiu, B., & Chen, S. (2004). Seasonal modulations in the eddy field of the South Pacific Ocean. *Journal of Physical Oceanography, 34*, 1515–1527.

Qiu, B., & Chen, S. (2005). Variability of the Kuroshio Extension jet, recirculation gyre and mesoscale eddies on decadal timescales. *Journal of Physical Oceanography, 35*, 2090–2103.

Qiu, B., & Chen, S. (2006). Decadal variability in the large-scale sea surface height field of the South Pacific Ocean: Observations and causes. *Journal of Physical*

Oceanography, 36, 1751–1762.

Qiu, B., & Chen, S. (2010). Interannual-to-decadal variability in the bifurcation of the North Equatorial Current off the Philippines. *Journal of Physical Oceanography, 40*, 2525–2538.

Qiu, B., Chen, S., & Hacker, P. (2007a). Effect of mesoscale eddies on Subtropical Mode Water variability from the Kuroshio Extension System Study (KESS). *Journal of Physical Oceanography, 37*, 982–1000.

Qiu, B., Chen, S., Hacker, P., Hogg, N., Jayne, S., & Sasaki, H. (2008). The Kuroshio Extension northern recirculation gyre: Profiling float measurements and forcing mechanism. *Journal of Physical Oceanography, 38*, 1764–1779.

Qiu, B., Chen, S., & Kessler, W. S. (2009). Source of the 70-day mesoscale eddy variability in the Coral Sea and the North Fiji Basin. *Journal of Physical Oceanography, 39*, 404–420.

Qiu, B., & Joyce, T. M. (1992). Interannual variability in the mid- and low-latitude western North Pacific. *Journal of Physical Oceanography, 22*, 1062–1079.

Qiu, B., & Lukas, R. (1996). Seasonal and interannual variability of the North Equatorial Current, the Mindanao Current and the Kuroshio along the Pacific western boundary. *Journal of Geophysical Research, 101*, 12,315–12,330.

Qiu, B., & Miao, W. (2000). Kuroshio path variations south of Japan: Bimodality as a self-sustained internal oscillation. *Journal of Physical Oceanography, 30*, 2124–2137.

Qiu, B., Schneider, N., & Chen, S. (2007b). Coupled decadal variability in the North Pacific: An observationally-constrained idealized model. *Journal of Climate, 20*, 3602–3620.

Qiu, B., Toda, T., & Imasato, N. (1990). On Kuroshio front fluctuations in the East China Sea using satellite and in-situ observational data. *Journal of Geophysical Research, 95*, 18,191–18,204.

Quadfasel, D., & Schott, F. (1982). Water-mass distributions at intermediate layers off the Somali coast during the onset of the southwest monsoon. *Journal of Physical Oceanography, 12*, 1358–1372.

Quadfasel, D., & Schott, F. (1983). Southward subsurface flow below the Somali Current. *Journal of Geophysical Research, 33*, 1307–1312.

Quartly, G. D., & Srokosz, M. A. (1993). Seasonal variations in the region of the Agulhas Retroflection: Studies with Geosat and FRAM. *Journal of Physical Oceanography, 23*, 2107–2124.

Read, J. F., & Pollard, R. T. (1993). Structure and transport of the Antarctic Circumpolar Current and Agulhas Return Current at 40°E. *Journal of Geophysical Research, 98,* 12,281–12,295.

Reason, C. J. C. (2001). Evidence for the influence of the Agulhas Current on regional atmospheric circulation patterns. *Journal of Climate, 14,* 2769–2778.

Reid, J. L. (1997). On the total geostrophic circulation of the Pacific Ocean: Flow pattern, tracers, and transports. *Progress in Oceanography, 39,* 263–352.

Richardson, P. L. (2007). Agulhas leakage into the Atlantic estimated with subsurface floats and surface drifters. *Deep-Sea Research I, 54,* 1361–1389.

Ridderinkhof, H., van der Werf, P. M., Ullgren, J. E., van Aken, H. M., van Leeuwen, P. J., & de Ruijter, W. P. M. (2010). Seasonal and interannual variability in the Mozambique Channel from moored current observations. *Journal of Geophysical Research, 115,* C06010, doi:10.1029/2009JC005619.

Ridgway, K. R. (2007). Long-term trend and decadal variability of the southward penetration of the East Australian Current. *Geophysical Research Letters, 34,* L13613, doi:10.1029/2007GL030393.

Ridgway, K. R., & Dunn, J. R. (2003). Mesoscale structure of the mean East Australian Current system and its relationship with topography. *Progress in Oceanography, 56,* 189–222.

Ridgway, K. R., & Dunn, J. R. (2007). Observational evidence for a Southern Hemisphere oceanic supergyre. *Geophysical Research Letters, 34,* L13612, doi:10.1029/2007GL030392.

Ridgway, K. R., & Godfrey, J. S. (1994). Mass and heat budgets in the East Australian Current: A direct approach. *Journal of Geophysical Research, 99,* 3231–3248.

Ridgway, K. R., & Godfrey, J. S. (1996). Long-term temperature and circulation changes off eastern Australia. *Journal of Geophysical Research, 101,* 3615–3627.

Ridgway, K. R., & Godfrey, J. S. (1997). Seasonal cycle of the East Australian Current. *Journal of Geophysical Research, 102,* 22,921–22,936.

Rio, M.-H., & Hernandez, F. (2004). A mean dynamic topography computed over the world ocean from altimetry, in situ measurements, and a geoid model. *Journal of Geophysical Research, 109,* C12032, doi:10.1029/2003JC002226.

Risien, C. M., & Chelton, D. B. (2008). A global climatology of surface wind and wind stress fields from eight years of QuikSCAT scatterometer data. *Journal of Physical Oceanography, 38,* 2379–2413.

Roemmich, D. (2007). Super spin in the southern seas. *Nature*, 449, 34–35.

Roemmich, D., & Gilson, J. (2001). Eddy transport of heat and thermocline waters in the North Pacific: A key to interannual/decadal climate variability? *Journal of Physical Oceanography, 31*, 675–687.

Roemmich, D., Gilson, J., Davis, R., Sutton, P., & Wijffels, S. (2007). Decadal spin-up of the South Pacific subtropical gyre. *Journal of Physical Oceanography, 37*, 162–173.

Roemmich, D., Gilson, J., Willis, J., Sutton, P., & Ridgway, K. (2005). Closing the time-varying mass and heat budgets for large ocean areas: The Tasman box. *Journal of Climate, 18*, 2330–2343.

Roemmich, D., & Sutton, P. (1998). The mean and variability of ocean circulation past northern New Zealand: Determining the representativeness of hydrographic climatologies. *Journal of Geophysical Research, 193*, 13,041–13,054.

Rossby, T. (1996). The North Atlantic Current and surrounding waters: At the crossroads. *Review of Geophysics, 34*, 463–481, doi:10.1029/96RG02214.

Rossby, T., & Benway, R. L. (2000). Slow variations in mean path of the Gulf Stream east of Cape Hatteras. *Geophysical Research Letters, 27*, 117–120.

Rossby, T., Flagg, C. N., & Donohue, K. (2005). Interannual variations in upper-ocean transport by the Gulf Stream and adjacent waters between New Jersey and Bermuda. *Journal of Marine Research, 63*, 203–226.

Rossby, T., Flagg, C., & Donohue, K. (2010). On the variability of Gulf Stream transport from seasonal to decadal timescales. *Journal of Marine Research, 68*, 503–522, doi:10.1357/002224010794657128.

Rouault, M., Lee-Thorp, A. M., & Lutjeharms, J. R. E. (2000). The atmospheric boundary layer above the Agulhas Current during along-current winds. *Journal of Physical Oceanography, 30*, 40–50.

Rouault, M., White, S. A., Reason, C. J. C., Lutjeharms, J. R. E., & Jobard, I. (2002). Ocean–atmosphere interaction in the Agulhas Current region and a South African extreme weather event. *Weather Forecast, 17*, 655–669.

Rypina, I. I., Pratt, L. J., & Lozier, M. S. (2011). Near-surface transport pathways in the North Atlantic Ocean: Looking for throughput from the subtropical to the subpolar gyre. *Journal of Physical Oceanography, 41*, 911–925.

Samelson, R. M. (1992). Fluid exchange across a meandering jet. *Journal of Physical Oceanography, 22*, 431–444.

Saraceno, M., Provost, C., Piola, A. R., Bava, J., & Gagliardini, A. (2004). Brazil

Malvinas Frontal System as seen from 9 years of advanced very high resolution radiometer data. *Journal of Geophysical Research, 109,* C05027, doi:10.1029/2003JC002127.

Sato, O. T., & Rossby, T. (1995). Seasonal and low frequency variability in dynamic height anomaly and transport of the Gulf Stream. *Deep-Sea Research, 42,* 149–164.

Schmitz, W. J. (1996). *On the world ocean circulation: Volume I: Some global features/North Atlantic circulation*. Woods Hole Oceanographic Institution Technical Report, WHOI-96-03, Woods Hole, MA, 141 pp.

Schmitz, W. J., & McCartney, M. S. (1993). On the North Atlantic circulation. *Review of Geophysics, 31*, 29–49, doi:10.1029/92RG02583.

Schmitz, W. J., & Richardson, P. L. (1991). On the sources of the Florida Current. *Deep-Sea Research, 38*, S379–S409.

Schoenefeldt, R., & Schott, F. A. (2006). Decadal variability of the Indian Ocean cross-equatorial exchange in SODA. *Geophysical Research Letters, 33,* L08602, doi:10.1029/2006GL025891.

Schott, F. A., & Fischer, J. (2000). Winter monsoon circulation of the northern Arabian Sea and Somali Current. *Journal of Geophysical Research, 105,* 6359–6376.

Schott, F., Fischer, J., Gartenicht, U., & Quadfasel, D. (1997). Summer monsoon response of the northern Somali Current, 1995. *Geophysical Research Letters, 24*, 2565–2568.

Schott, F., Fischer, J., & Stramma, L. (1998). Transports and pathways of the upper-layer circulation in the western tropical Atlantic. *Journal of Physical Oceanography, 28*, 1904–1928.

Schott, F. A., Lee, T. N., & Zantopp, R. (1988). Variability of structure and transport of the Florida Current in the period range of days to seasonal. *Journal of Physical Oceanography, 18,* 1209–1230.

Schott, F. A., & McCreary, J. P. (2001). The monsoon circulation of the Indian Ocean. *Progress in Oceanography, 51,* 1–123.

Schott, F., Swallow, J. C., & Fieux, M. (1990). The Somali Current at the equator: Annual cycle of currents and transports in the upper 1000 m and connection to neighbouring latitudes. *Deep-Sea Research, 37,* 1825–1848.

Schott, F. A., & Zantopp, R. J. (1985). Florida Current: Seasonal and interannual variability. *Science, 227,* 308–311.

Schott, F., Zantopp, R., Stramma, L., Dengler, M., Fischer, J., & Wibaux, M. (2004).

Circulation and deep water export at the western exit of the subpolar North Atlantic. *Journal of Physical Oceanography, 34*, 817–843.

Schouten, M. W., de Ruijter, W. P. M., & van Leeuwen, P. J. (2002). Upstream control of Agulhas Ring shedding. *Journal of Geophysical Research*, *107*, 3109, doi:10.1029/2001JC000804.

Schouten, M. W., de Ruijter, W. P. M., van Leeuwen, P. J., & Lutjeharms, J. R. E. (2000). Translation, decay and splitting of Agulhas rings in the southeastern Atlantic Ocean. *Journal of Geophysical Research*, *105*, 21,913–21,925.

Send, U., & Co-Authors (2010). A global boundary current circulation observing network. In J. Hall, D.E. Harrison & D. Stammer (Eds.), *Proceedings of OceanObs'09: Sustained Ocean Observations and Information for Society (Vol. 2)*, Venice, Italy, 21–25 September 2009, ESA Publication WPP-306, doi:10.5270/OceanObs09.cwp.78.

Seo, H., Murtugudde, R., Jochum, M., & Miller, A. J. (2008). Modeling of mesoscale coupled ocean–atmosphere interaction and its feedback to ocean in the western Arabian Sea. *Ocean Modelling*, *25*, 120–131.

Shaw, P.-T., & Rossby, H. T. (1984). Towards a Lagrangian description of the Gulf Stream. *Journal of Physical Oceanography, 14*, 528–540.

Shukla, J. (1975). Effect of Arabian Sea-surface temperature anomaly on Indian summer monsoon: A numerical experiment with the GFDL model. *Journal of the Atmospheric Sciences*, *32*, 503–511.

Sijp W. P., & England, M. H. (2009). Southern Hemisphere westerly wind control over the ocean's thermohaline circulation. *Journal of Climate*, *22*, 1277–1286.

Smith, R. D., Maltrud, M. E., Bryan, F. O., & Hecht, M. W. (2000). Numerical simulation of the North Atlantic Ocean at 1/10°. *Journal of Physical Oceanography, 30*, 1532–1561.

Song, T., & Rossby, T. (1995). Lagrangian studies of fluid exchange between the Gulf Stream and surrounding patterns. *Journal of Physical Oceanography*, *25*, 46–63.

Spadone, A., & Provost, C. (2009). Variations in the Malvinas Current volume transport since 1992. *Journal of Geophysical Research*, *114*, C02002. doi:10.1029/2008JC004882.

Spall, M. A. (1996a). Dynamics of the Gulf Stream/Deep Western Boundary Current crossover, Part I: Entrainment and recirculation. *Journal of Physical Oceanography, 26*, 2152–2168.

Spall, M. A. (1996b). Dynamics of the Gulf Stream/Deep Western Boundary Current

crossover, Part II: Low frequency internal oscillations. *Journal of Physical Oceanography, 26,* 2169–2182.

Speich, S., Blanke, B., de Vries, P., Drijfhout, S., Döös, K., Ganachaud, A., & Marsh, R. (2002). Tasman leakage: A new route in the global ocean conveyor belt. *Geophysical Research Letters, 29*, 1416, doi:10.1029/2001GL014586.

Speich, S., Lutjeharms, J. R. E., Penven, P., & Blanke, B. (2006). Role of bathymetry in Agulhas Current configuration and behavior. *Geophysical Research Letters, 33,* L23611, doi:10.1029/2006GL027157.

Stanton, B. R. (2001). Estimating the East Auckland Current transport from model winds and the Island Rule. *New Zealand Journal of Marine and Freshwater Research, 35,* 531–540.

Stanton, B., Roemmich, D., & Kosro, M. (2001). A shallow zonal jet south of Fiji. *Journal of Physical Oceanography, 31*, 3127–3130.

Stanton, B., & Sutton, P. (2003). Velocity measurements in the East Auckland Current north-east of North Cape, New Zealand. *New Zealand Journal of Marine and Freshwater Research, 37*, 195–204.

Stommel, H. (1948). The westward intensification of wind-driven ocean currents. *Transactions, American Geophysical Union, 29*, 202–206.

Stommel, H. (1965). *The Gulf Stream: A physical and dynamical description, second edition.* University of California Press, Berkeley, 248 pp.

Stommel, H. M., & Arons, A. (1960a). On the abyssal circulation of the World Ocean – I. Stationary planetary flow patterns on a sphere. *Deep-Sea Research, 6*, 140–154.

Stommel, H. M., & Arons, A. (1960b). On the abyssal circulation of the World Ocean – II. An idealized model of the circulation pattern and amplitude in oceanic basins. *Deep-Sea Research, 6*, 217–233.

Stommel, H., & Yoshida, K. (Eds.) (1972). *Kuroshio: Its physical aspects*. University of Tokyo Press, Tokyo, 517 pp.

Stramma, L., Fischer, J., & Reppin, J. (1995). The North Brazil Undercurrent. *Deep-Sea Research, 42*, 773–795.

Stramma, L., Ikeda, Y., & Peterson, R. G. (1990). Geostrophic transport in the Brazil Current region north of 20°S. *Deep-Sea Research, 37*, 1875–1886.

Stramma, L., & Lutjeharms, J. R. E. (1997). The flow field of the subtropical gyre of the South Indian Ocean. *Journal of Geophysical Research, 102*, 5513–5530.

Sugimoto, S., & Hanawa, K. (2010). Impact of Aleutian Low activity on the STMW formation in the Kuroshio recirculation gyre region. *Geophysical Research*

Letters, 37, L03606, doi:10.1029/2009GL041795.

Sugimoto, T., Kimura, S., & Miyaji, K. (1988). Meander of the Kuroshio front and current variability in the East China Sea. *Journal of the Oceanographical Society of Japan, 44*, 125–135.

Sutton, P. (2001). Detailed structure of the Subtropical Front over Chatham Rise, east of New Zealand. *Journal of Geophysical Research, 106*, 31,045–31,056.

Swallow, J. C., & Bruce, J. G. (1966). Current measurements off the Somali coast during the southwest monsoon of 1964. *Deep-Sea Research, 13*, 861–888

Swallow, J. C., Molinari, R. L., Bruce, J. G., Brown, O. B., & Evans, R. H. (1983). Development of near-surface flow pattern and water mass distribution in the Somali Basin in response to the southwest monsoon of 1979. *Journal of Physical Oceanography, 13*, 1398–1415.

Taguchi, B., Xie, S.-P., Schneider, N., Nonaka, M., Sasaki, H., & Sasai, Y. (2007). Decadal variability of the Kuroshio Extension: Observations and an eddy-resolving model hindcast. *Journal of Climate, 20*, 2357–2377.

Takahashi, T., & Co-Authors (2009). Climatological mean and decadal changes in surface ocean pCO_2, and net sea-air CO_2 flux over the global oceans. *Deep Sea Research II, 56*, 554–577, Doi: 10.1016/j.dsr2.2008.12.009.

Talley, L. D., Pickard, G. L., Emery, W. J., & Swift, J. H. (2011). *Descriptive physical oceanography: An introduction, sixth edition*. Elsevier, London, 555 pp.

Tansley, C. E., & Marshall, D. P. (2000). On the influence of bottom topography and the Deep Western Boundary Current on Gulf Stream separation. *Journal of Marine Research, 58*, 297–325.

Thompson, J. D., & Schmitz, W. J. (1989). A limited-area model of the Gulf Stream: Design, initial experiments, and model-data intercomparison. *Journal of Physical Oceanography, 19*, 791–814.

Tillburg, C. E., Hurlburt, H. E., O'Brien, J. J., & Shriver, J. F. (2001). The dynamics of the East Australian Current System: The Tasman Front, the East Auckland Current, and the East Cape Current. *Journal of Physical Oceanography, 31*, 2917–2943.

Trenberth, K. E., & Caron, J. M. (2001). Estimates of meridional atmosphere and ocean heat transports. *Journal of Climate, 14*, 3433–3443.

Tsugawa, M., & Hasumi, H. (2010). Generation and growth mechanism of the Natal Pulse. *Journal of Physical Oceanography, 40*, 1597–1612.

Tsujino, H., Usui, N., & Nakano, H. (2006). Dynamics of Kuroshio path variations

in a high-resolution GCM. *Journal of Geophysical Research, 111*, C11001, doi:10.1029/2005JC003118.

Uchida, H., & Imawaki, S. (2008). Estimation of the sea level trend south of Japan by combining satellite altimeter data with in situ hydrographic data. *Journal of Geophysical Research, 113*, C09035, doi:10.1029/2008JC004796.

Uddstrom, M. J., & Oien, N. A. (1999). On the use of high-resolution satellite data to describe the spatial and temporal variability of sea surface temperatures in the New Zealand region. *Journal of Geophysical Research, 104*, 20,729–20,751.

Usui, N., Tsujino, H., Nakano, H., & Fujii, Y. (2008). Formation process of the Kuroshio large meander in 2004. *Journal of Geophysical Research, 113*, C08047, doi:10.1029/2007JC004675.

van Aken, H. M., van Veldhoven, A. K., Veth, C., de Ruijter, W. P. M., van Leeuwen, P. J., Drijfhout, S. S., Whittle, C. P., & Rouault, M. (2003). Observations of a young Agulhas ring, Astrid, during MARE in March 2000. *Deep-Sea Research II, 50*, 167–195.

van Leeuwen, P. J., & de Ruijter, W. P. M. (2009). On the steadiness of separating meandering currents. *Journal of Physical Oceanography, 39*, 437–448.

van Sebille, E., Biastoch, A., van Leeuwen, P. J., & de Ruijter, W. P. M. (2009). A weaker Agulhas Current leads to more Agulhas leakage. *Geophysical Research Letters, 36*, L03601, doi:10.1029/2008GL036614.

van Sebille, E., van Leeuwen, P. J., Biastoch, A., & de Ruijter, W. P. M. (2010). Flux comparison of Eulerian and Lagrangian estimates of Agulhas leakage: A case study using a numerical model. *Deep-Sea Research I, 57*, 319–327.

Vecchi, G. A., Sahng-Ping, X., & Fischer, A. S. (2004). Ocean–atmosphere covariability in the western Arabian Sea. *Journal of Climate*, *17*, 1213–1224.

Veronis, G. (1973). Model of world ocean circulation: I. Wind-driven, two-layer. *Journal of Marine Research*, *31,* 228–288.

Veronis, G. (1978). Model of world ocean circulation: III. Thermally and wind driven. *Journal of Marine Research*, *36*, 1–44.

Vivier, F., Kelly, K. A., & Thompson, L. (2002). Heat budget in the Kuroshio Extension region, 1993–1999. *Journal of Physical Oceanography, 32*, 3436–3454.

Warren, B., Stommel, H., & Swallow, J. C. (1966). Water masses and patterns of flow in the Somali Basin during the southwest monsoon of 1964. *Deep-Sea Research, 13,* 825–860.

Webb, D. J. (2000). Evidence for shallow zonal jets in the South Equatorial Current region of the southwest Pacific. *Journal of Physical Oceanography, 30*, 706–720.

Weijer, W., de Ruijter, W. P. M., Sterl, A., & Drijfhout, S. S. (2002). Response of the Atlantic overturning circulation to South Atlantic sources of buoyancy. *Global and Planetary Change, 34,* 293–311.

Wijffels, S. E., Hall, M. M., Joyce, T., Torres, D. J., Hacker, P., & Firing, E. (1998). Multiple deep gyres of the western North Pacific: A WOCE section along 149°E. *Journal of Geophysical Research, 103*, 12,985–13,009.

Wirth, A., Willebrand, J., & Schott, F. (2002). Variability of the Great Whirl from observations and models. *Deep-Sea Research II, 49,* 1279–1295.

Witter, D. L., & Gordon, A. L. (1999). Interannual variability of South Atlantic circulation from four years of TOPEX/POSEIDON satellite altimeter observations. *Journal of Geophysical Research*, *104*, 20,927–20,948.

Woityra, W., & Rossby, T. (2008). Current broadening as a mechanism for anticyclogenesis at the Northwest Corner of the North Atlantic Current. *Geophysical Research Letters*, *35*, L05609, doi:10.1029/2007GL033063.

Worthington, L. V. (1976). *On the North Atlantic circulation*. The Johns Hopkins Oceanographic Studies, Vol. 6, Johns Hopkins University Press, Baltimore, Maryland, 110 pp.

Wyrtki, K. (1971). *Oceanographic atlas of the International Indian Ocean Expedition*. National Science Foundation, Washington, D. C., 531 pp.

Yasuda, I., Okuda, O., & Hirai M. (1992). Evolution of a Kuroshio warm-core ring – Variability of the hydrographic structure. *Deep-Sea Research, 39*, 131–161.

Yu, L., & Weller, R. A. (2007). Objectively analyzed air-sea heat fluxes for the global ice-free oceans (1981–2005). *Bulletin of the American Meteorological Society, 88*, 527–539.

Zemba, J. C., & McCartney, M. S. (1988). Transport of the Brazil Current: It's bigger than we thought. Abstract in: *Eos, Transactions, American Geophysical Union, 69,* 1237.

Zhang, D., Lee, T. N., Johns, W. E., Liu, C.-T., & Zantopp, R. (2001a). The Kuroshio east of Taiwan: Modes of variability and relationship to interior ocean mesoscale eddies. *Journal of Physical Oceanography, 31*, 1054–1074.

Zhang, H.-M., Prater, M. D., & Rossby, T. (2001b). Isopycnal Lagrangian statistics from the North Atlantic Current RAFOS float observations. *Journal of Geophysical Research, 106*, 13,817–13,836.

Zhang, R., & Vallis, G. K. (2007). The role of bottom vortex stretching on the path of the North Atlantic western boundary current and on the northern recirculation gyre. *Journal of Physical Oceanography, 37,* 2053–2080.

Zinke, J., Dullo, W.-C., Heiss, G. A., & Eisenhauer, A. (2004). ENSO and Indian Ocean subtropical dipole variability is recorded in a coral record off southwest Madagascar for the period 1659 to 1995. *Earth and Planetary Science Letters, 228,* 177–194.

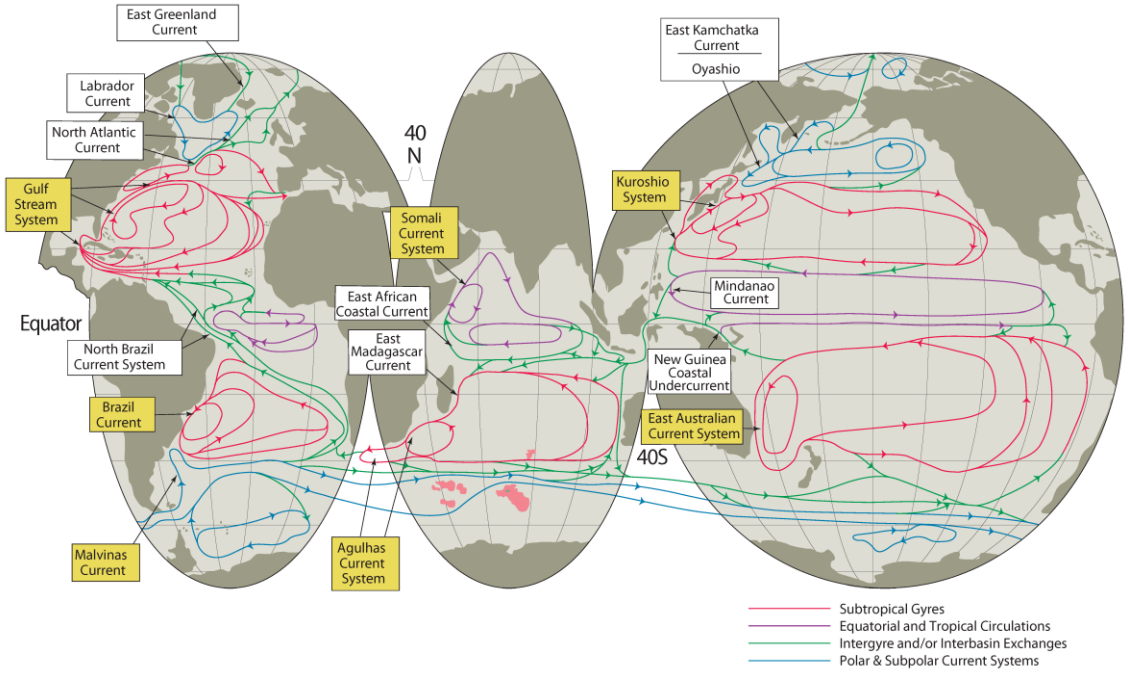

Figure 1.6 (This figure will not appear in this chapter but in Chapter 1.)
Schematic global summary of major currents in the upper-ocean, with labels for major WBCs (from Schmitz, 1996; Talley et al., 2011). Four kinds of colored lines indicate differences in characteristic regions and circulation mechanisms; notations are shown at the right-hand-side bottom.

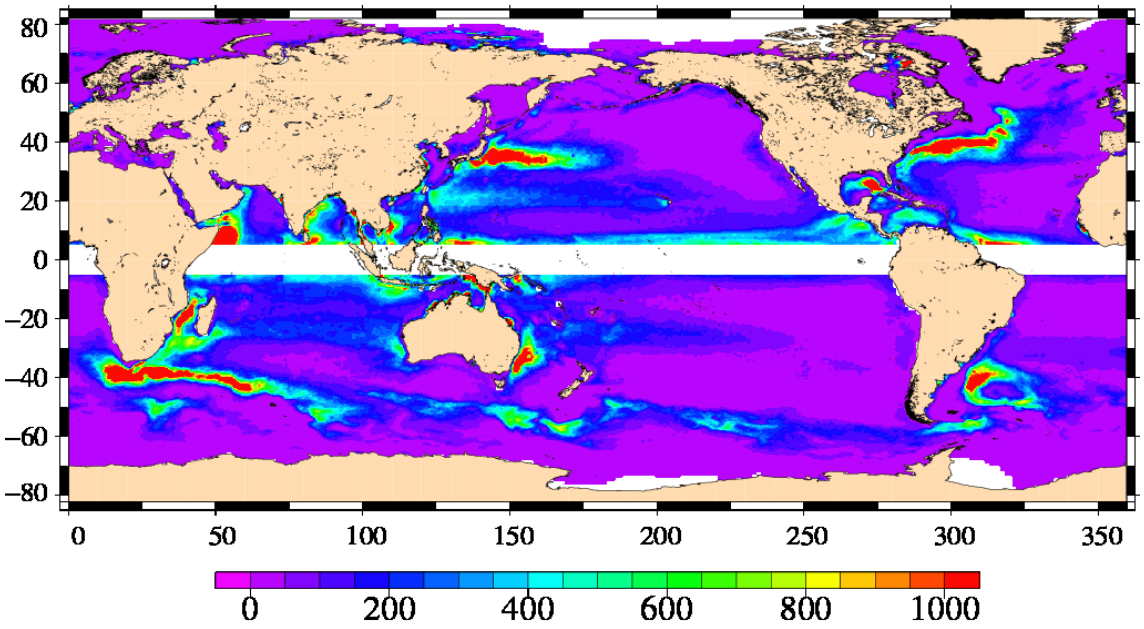

Figure 13.1

Global distribution of the climatological mean EKE (in $cm^2\ s^{-2}$) at the sea surface derived from satellite altimetry data obtained during 1993–2011. The equatorial regions are blank because the Coriolis parameter is too small for geostrophic velocities to be estimated accurately from altimetric SSH. From Ducet et al. (2000) and Dibarboure et al. (2011).

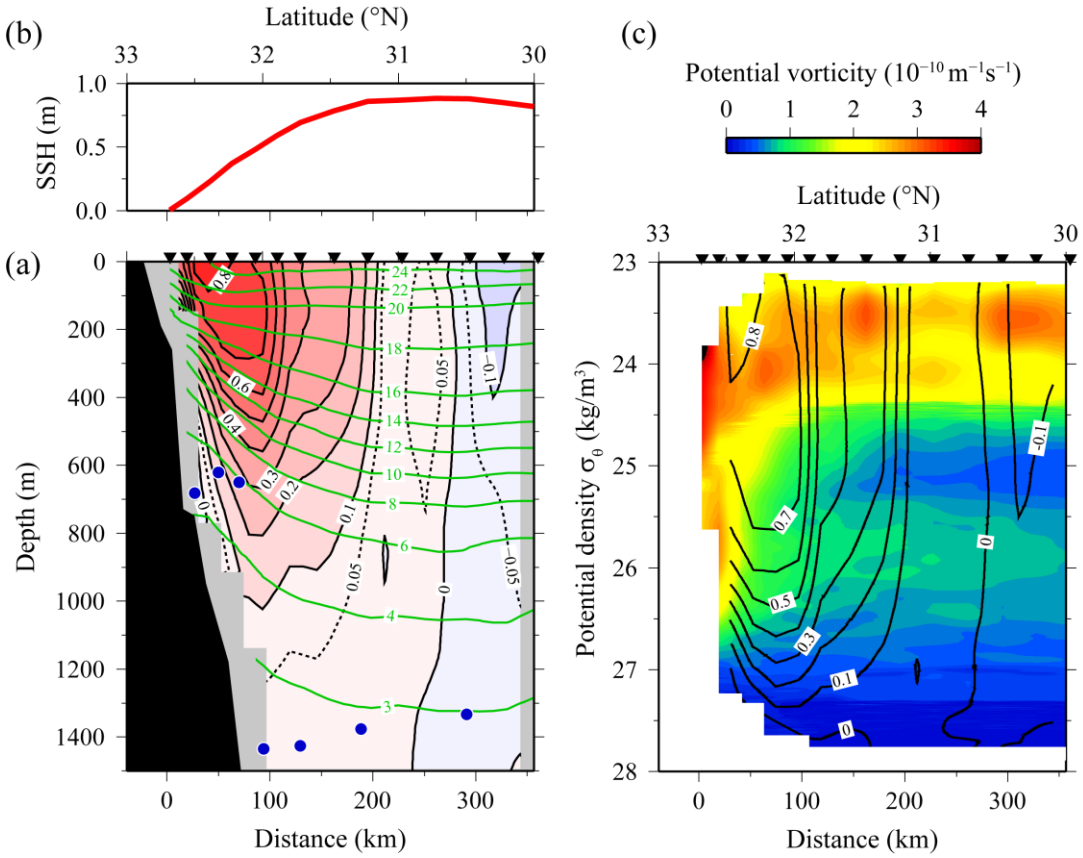

Figure 13.2

Vertical structure of the Kuroshio south of Japan. (a) Vertical section of temperature (in °C; green contours) and velocity (in m s^{-1}; positive, eastnortheastward; color shading with black contours), averaged over 2 years from October 1993 through November 1995. During that period, the Affiliated Surveys of the Kuroshio off Cape Ashizuri were carried out intensively (Uchida and Imawaki, 2008). Velocity is estimated from hydrographic data assuming geostrophy, being referred to observed velocities at locations shown by blue dots. Distance is directed offshore. (b) SSH profile relative to the coastal station, estimated from the surface velocity assuming geostrophy. (c) Section of potential vorticity (in m^{-1} s^{-1}; color shading; Beal et al., 2006) plotted in potential density σ_θ space. Overlaid are velocity contours (black) same as in (a); contours associated with the strong shear near the coast are omitted for the sake of visibility. Courtesy of Dr. Hiroshi Uchida.

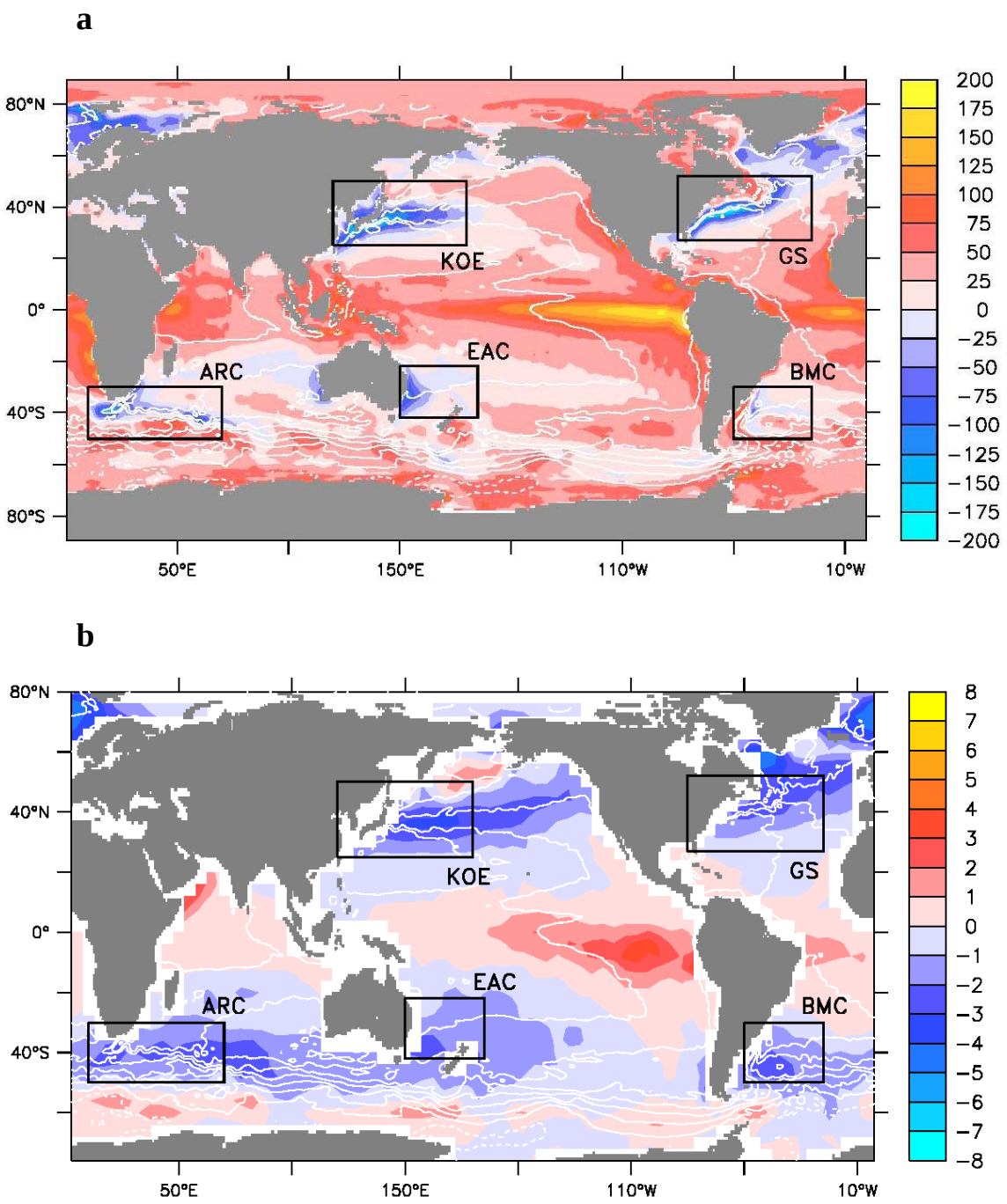

Figure 13.3

Global distribution of the climatological mean (a) latent plus sensible heat flux (in W m^{-2}; positive, atmosphere to ocean; Yu and Weller, 2007) and (b) CO_2 flux (in mol m^{-2} $year^{-1}$; positive, ocean to atmosphere; Takahashi et al., 2009) at the sea surface; the latter is for the reference year 2000 (non-El Niño conditions). White contours indicate mean sea surface dynamic height (Rio and Hernandez, 2004). ARC, Agulhas Return Current; KOE,

Kuroshio–Oyashio Extension; EAC, East Australian Current; GS, Gulf Stream; and BMC, Brazil/Malvinas Current. From Cronin et al. (2010).

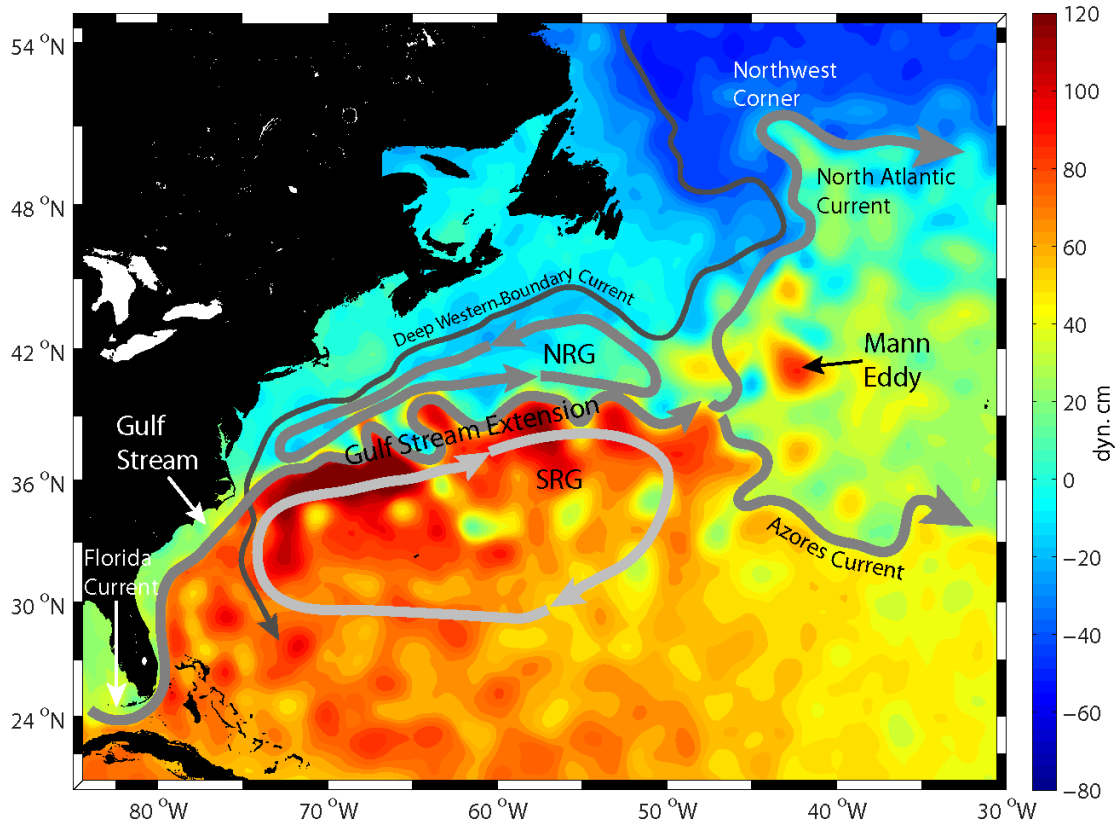

Figure 13.4

Map of Absolute Dynamic Topography (in dynamic cm; color shading) on September 21, 2011 for the western North Atlantic from AVISO (Archiving, Validation, and Interpretation of Satellite Oceanographic Data) Web site (http://www.aviso.oceanobs.com/), with schematic of currents in the Gulf Stream System, including the Northern and Southern Recirculation gyres (NRG and SRG).

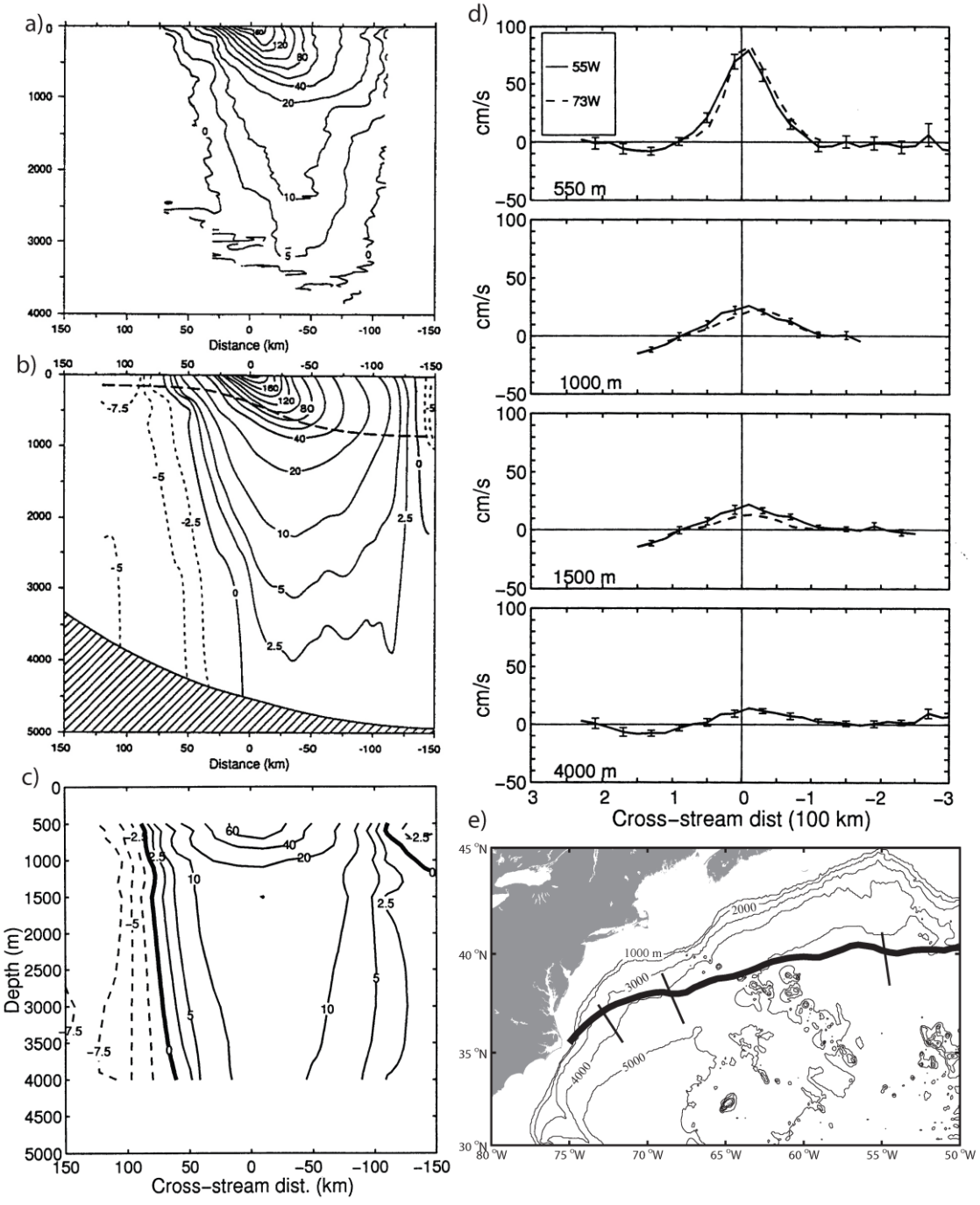

Figure 13.5

Sections of mean along-stream velocity (in cm s^{-1}) in stream-wise coordinates for three longitudes along the path of the GSE: (a) 73°W, (b) 68°W, and (c) 55°W. Downstream velocities are contoured with solid lines. Negative cross-stream distance is directed offshore. (d) Direct comparison of along-stream velocity (in cm s^{-1}) at 73°W and 55°W for four depths, showing similarity of peak speeds and cross-stream structure. Error bars show 95% confidence levels for the mean at 55°W. (e) Map showing locations of the

three sections depicted in (a)–(c). The mean GSE path is drawn as a wide black line. Panels (a) through (d): from Bower and Hogg (1996).

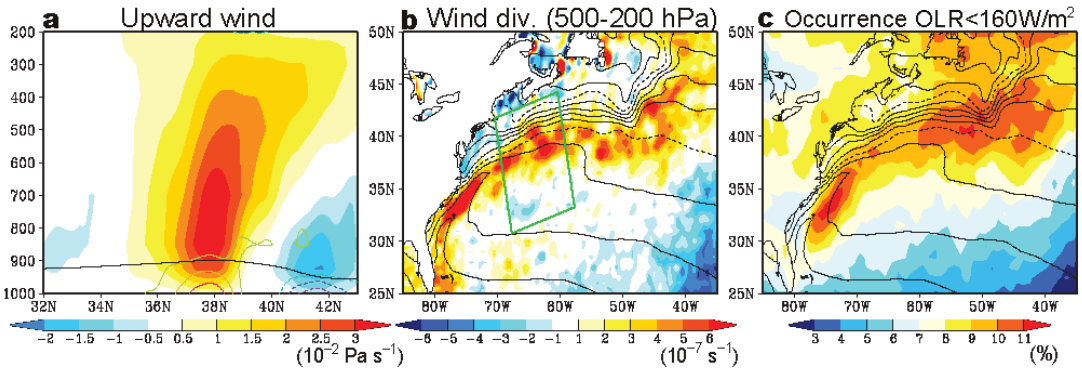

Figure 13.6

Annual climatology of (a) vertical wind velocity (upward positive; color), marine–atmospheric boundary layer height (black curve), and wind convergence (contours for ±1, 2, 3 × 10^{-6} s^{-1}) averaged in the along-front direction in the green box in (b), based on the ECMWF analysis; (b) upper tropospheric wind divergence averaged between 200 and 500 hPa (color); (c) occurrence frequency of daytime satellite-derived outgoing long-wave radiation levels lower than 160 W m^{-2} (color). Contours in (b) and (c) are for mean SST, with 2 °C contour interval and dashed contours for 10° and 20 °C. From Minobe et al. (2008).

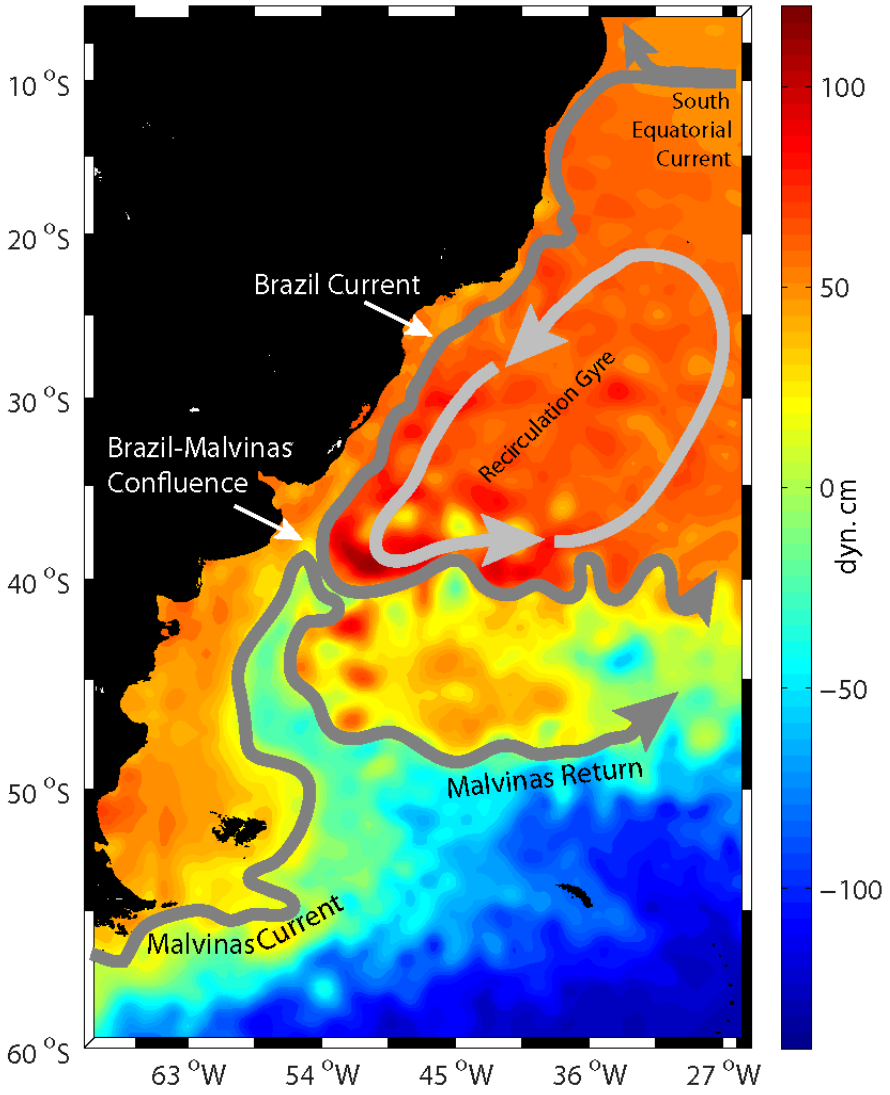

Figure 13.7

Map of Absolute Dynamic Topography (in dynamic cm; color shading) on December 22, 2010 for the western South Atlantic from AVISO Web site, with schematic of currents in the South Atlantic WBC system.

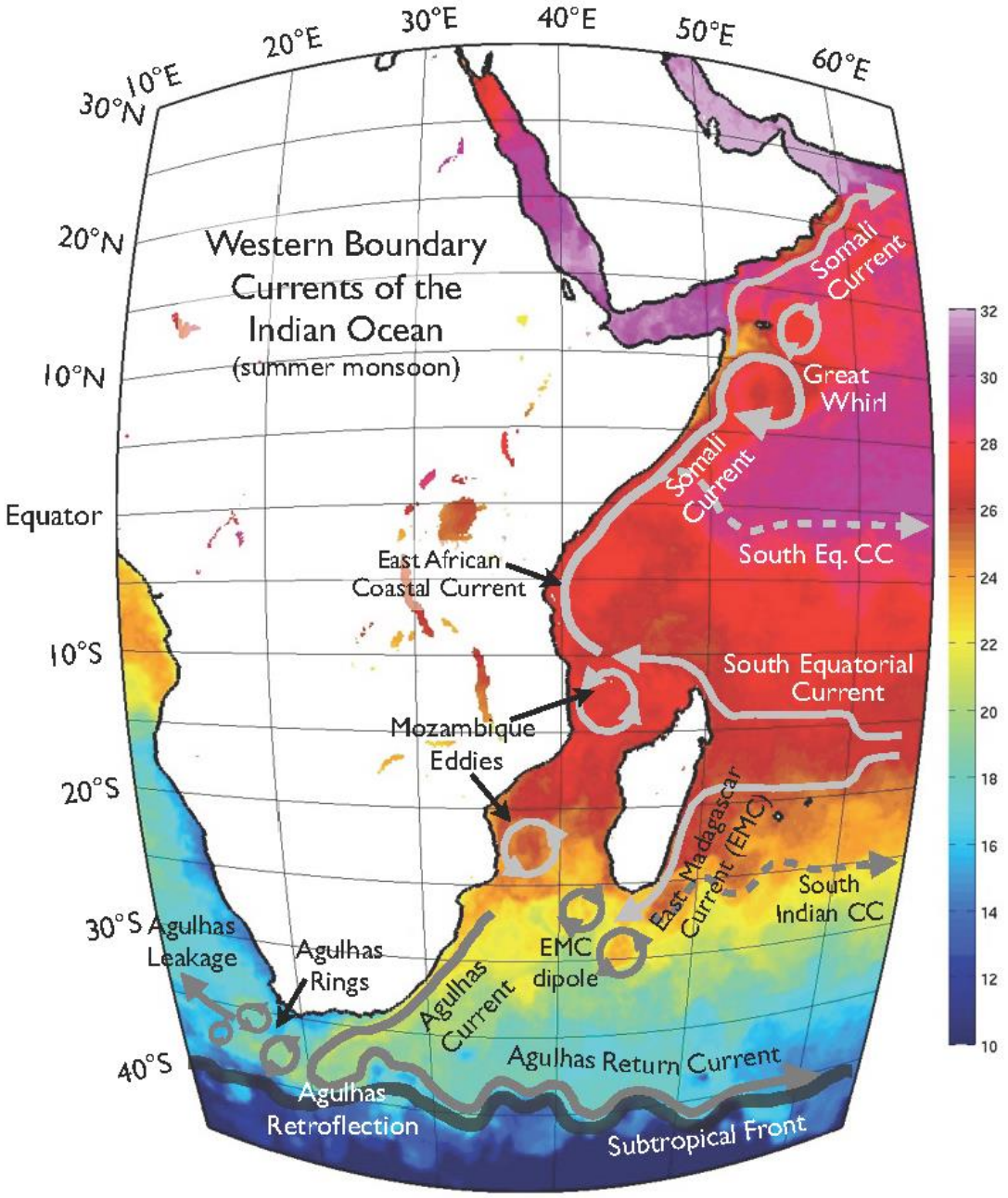

Figure 13.8

Schematic of the WBC system of the Indian Ocean, showing the Agulhas and Somali Currents, their sources and associated features, and the leakage of Agulhas waters into the Atlantic. SST (in °C; color shading) is for June 29, 2009 from the NAVOCEANO (United States Naval Oceanographic Office) Level 4 analysis, produced by interpolation of infrared and passive microwave observations, made available through the GHRSST (Group for High-Resolution Sea Surface Temperature) project (Donlon et al., 2007). CC, Countercurrent.

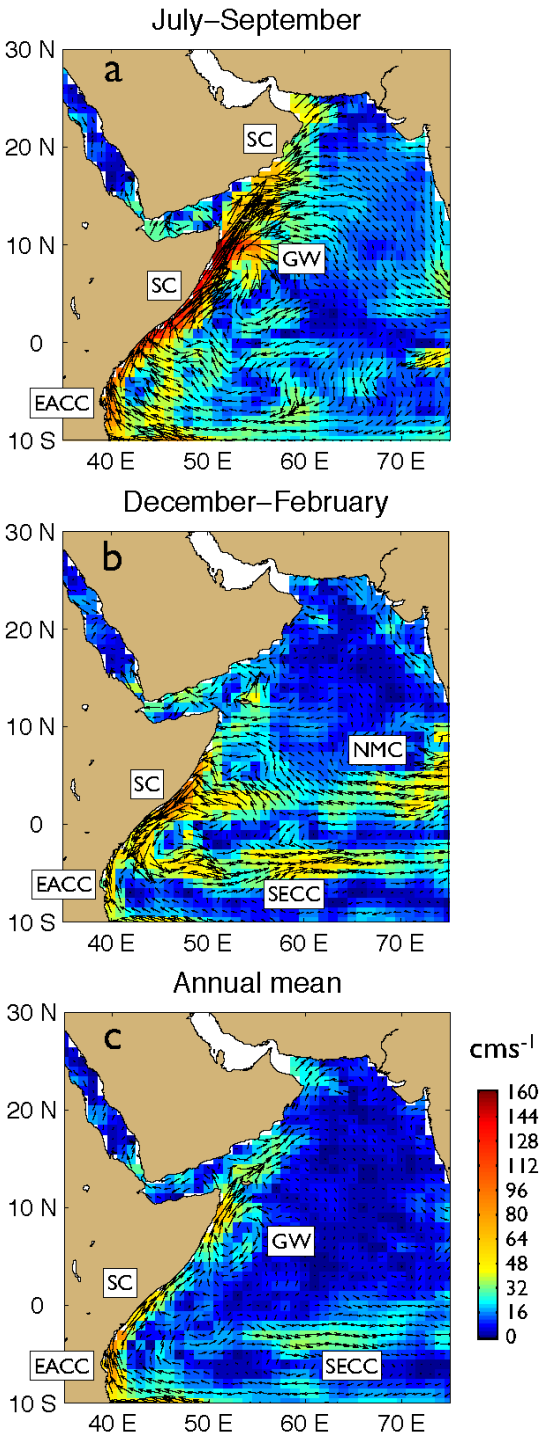

Figure 13.9

Surface currents of the Arabian Sea during (a) summer monsoon, (b) winter monsoon, and (c) annual mean, from the global drifter climatology (1993–2010). Color shading shows current speed (in cm s^{-1}), and arrows, current directions. Features are the Somali Current (SC), Great Whirl (GW), East African Coastal Current (EACC), North Monsoon Current (NMC), and

South Equatorial Counter Current (SECC). Data from http://www.aoml.noaa.gov/phod/dac/dac_meanvel.php (Lumpkin and Garraffo, 2005).

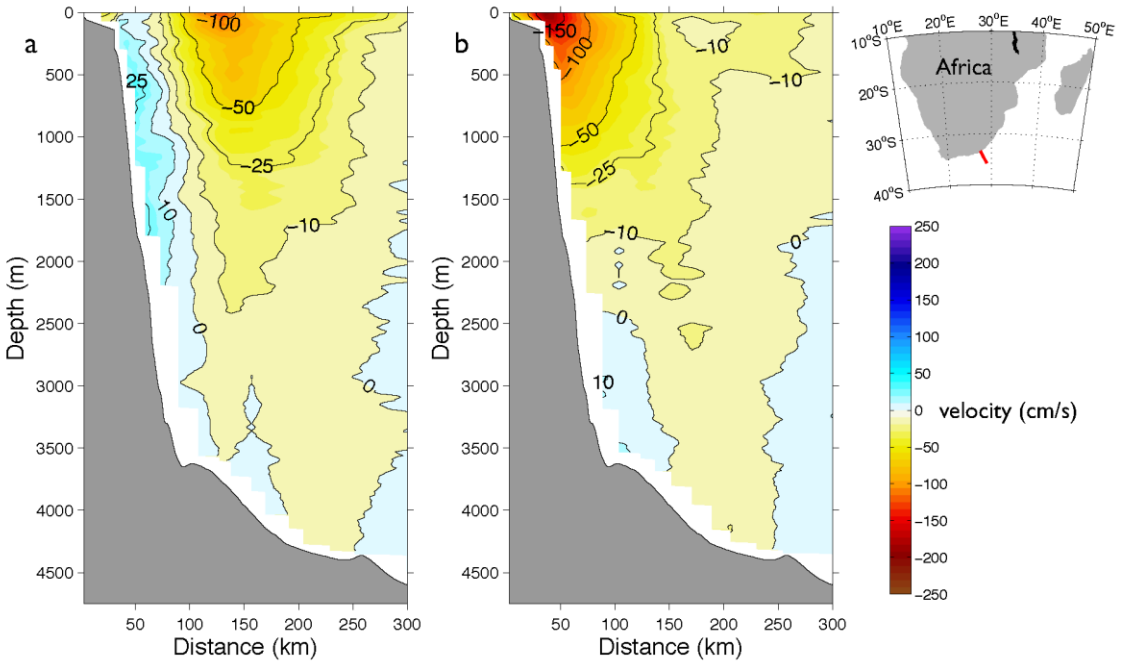

Figure 13.10

Velocity structure of the Agulhas Current near 34°S in (a) April 2010 during a solitary meander, when the current is located in offshore deepwater, and (b) November 2011, when the current is attached to the continental slope. Index map shows the position of the section. Velocity component (in cm s^{-1}; positive, eastnortheastward) perpendicular to the section is shown. Velocities were obtained from Lowered ADCP, during the Agulhas Current Time-series Experiment. From Beal and Bryden (1999).

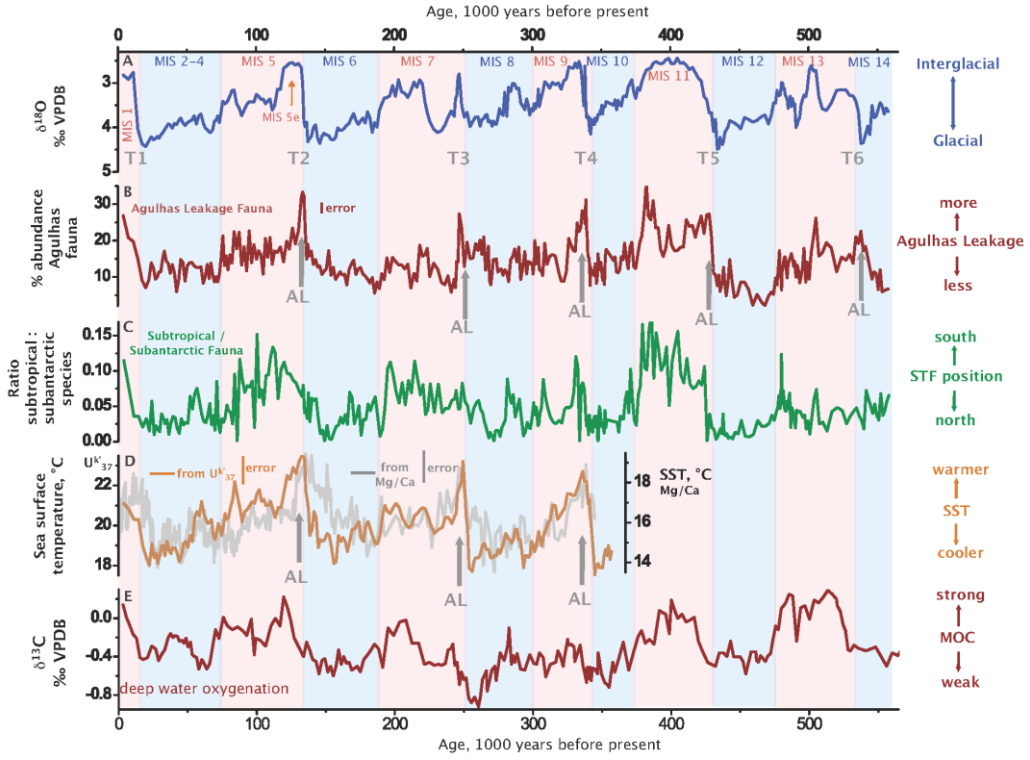

Figure 13.11

Paleoceanographic time series from the Agulhas leakage corridor spanning the last 570,000 year, adapted from Beal et al (2011). (a) Stable oxygen isotope profile, a proxy for glacial–interglacial variations in global climate. Marine isotope stages are labeled and highlighted by vertical blue/red shading. T1–T6 mark terminations of the past six glacial periods. (b) Abundance of tropical planktonic foraminiferal marker species, indicating maximum Agulhas leakage (AL) during glacial terminations. (c) Ratio of subtropical to subantarctic species, which are related to north–south migrations of the subtropical front. (d) SST derived from temperature-sensitive biomarkers $U^{k'}$ (brown line), and Mg/Ca ratios (gray line). Both reconstructions show maximum SST during glacial terminations, coinciding with Agulhas leakage events. (e) Benthic $\delta^{13}C$ from deep Pacific, thought to be linked to ocean ventilation and the strength of the Atlantic overturning circulation. Overturning strength appears to increase at each glacial termination, leading to the hypothesis that Agulhas leakage may trigger changes. From Beal et al. (2011).

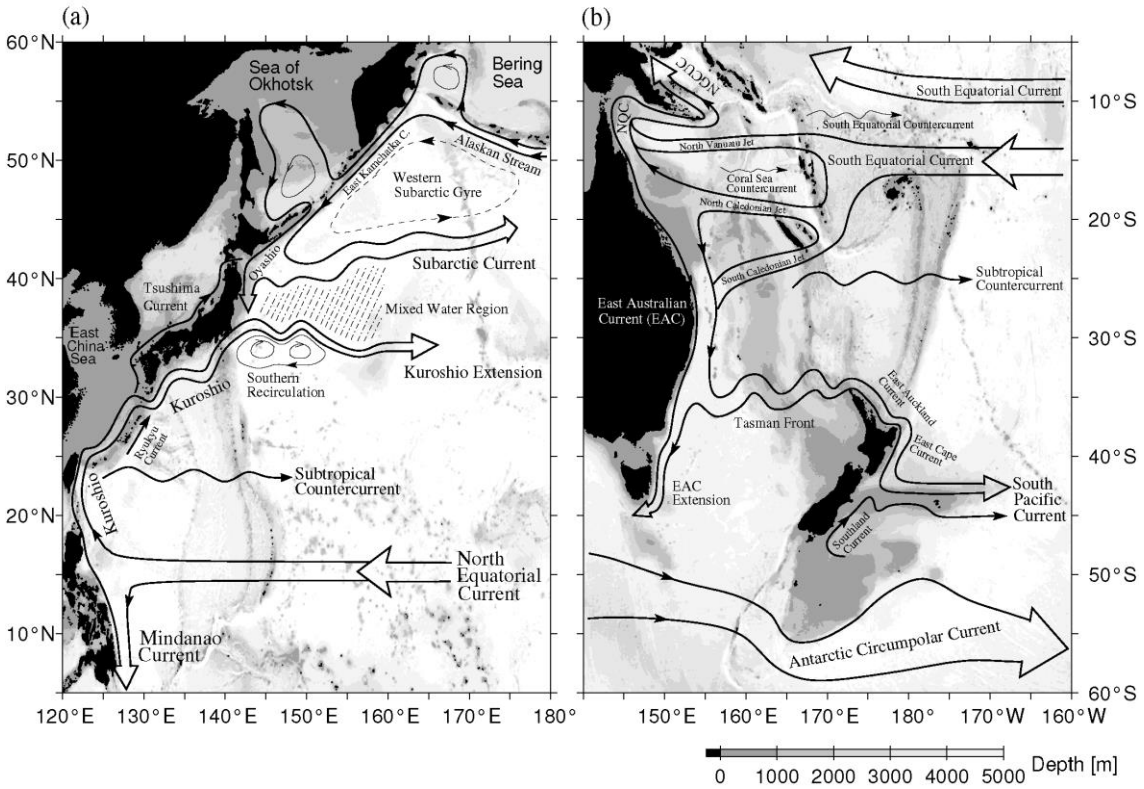

Figure 13.12

Schematic surface circulation pattern in (a) the western North Pacific and (b) the western South Pacific. Gray shading shows depth (in m). Abbreviations in (a) are: LZ, Luzon Strait; TS, Tokara Strait; and RIC, Ryukyu Island Chain, and in (b) are: NGCUC, New Guinea Coastal Undercurrent; NQC, North Queensland Current; QP, Queensland Plateau; NC, New Caledonia; LHR, Lord Howe Rise; NR, Norfolk Ridge; and NB, Norfolk Basin.

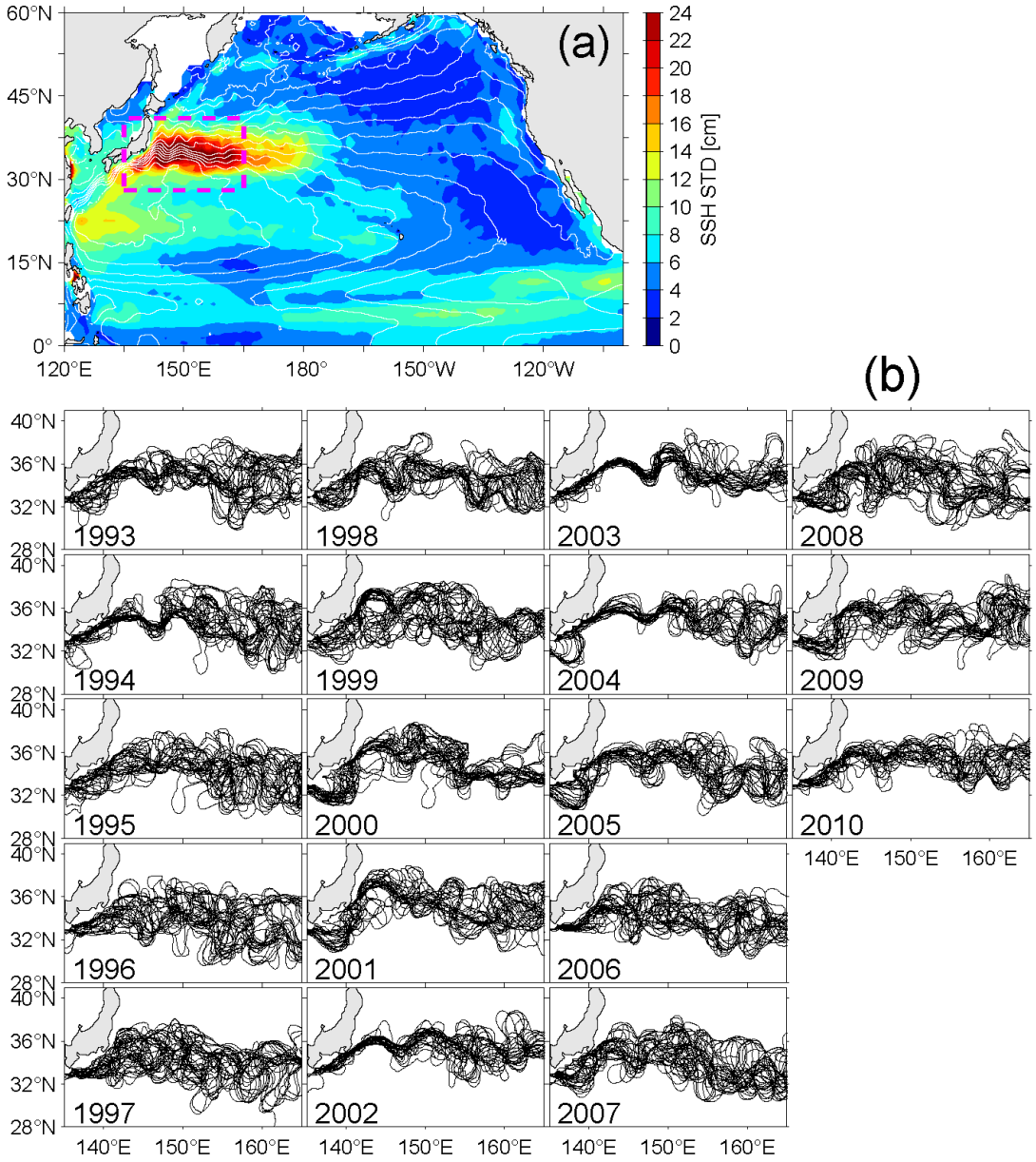

Figure 13.13

(a) Standard deviation of interannually varying SSH signals (in cm; color shading) in the North Pacific from October 1992 to December 2010. White contours denote the mean SSH field with contour intervals at 0.1 m. (b) Yearly paths of the Kuroshio and KE defined by the 1.7 m contours in the weekly SSH fields. Paths are plotted every 14 days. Adapted from Qiu and Chen (2005).

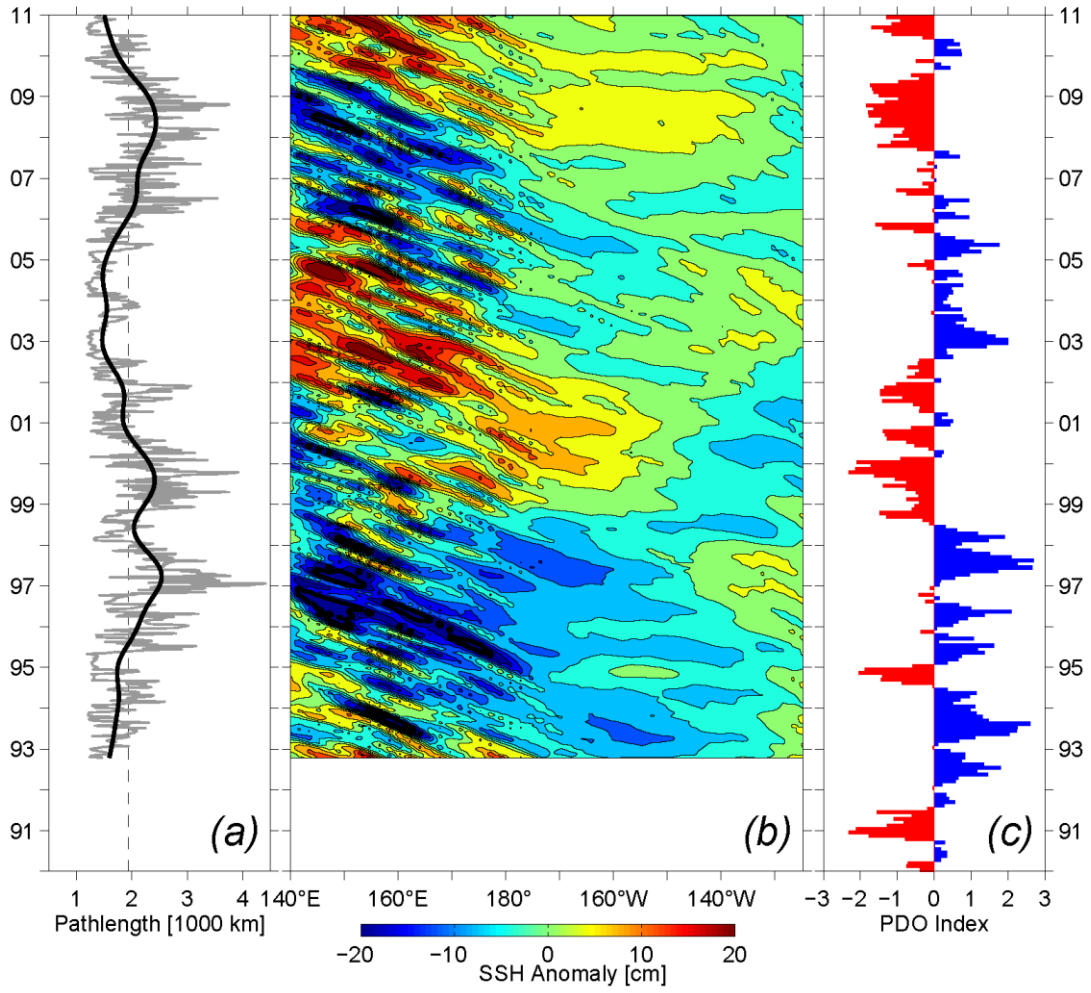

Figure 13.14

(a) Time series of the KE jet path length (in km) integrated from 141° to 153°E. A small value indicates a stable KE jet and a large value, a convoluted and dynamically unstable KE jet (see Figure 13.13). Gray line shows the weekly time series and black line shows the low-pass filtered time series. (b) SSH anomalies (in cm; color shading) versus time along the zonal band of 32–34°N from the AVISO satellite altimeter data. (c) PDO index versus time from http://jisao.washington.edu/pdo/PDO.latest.

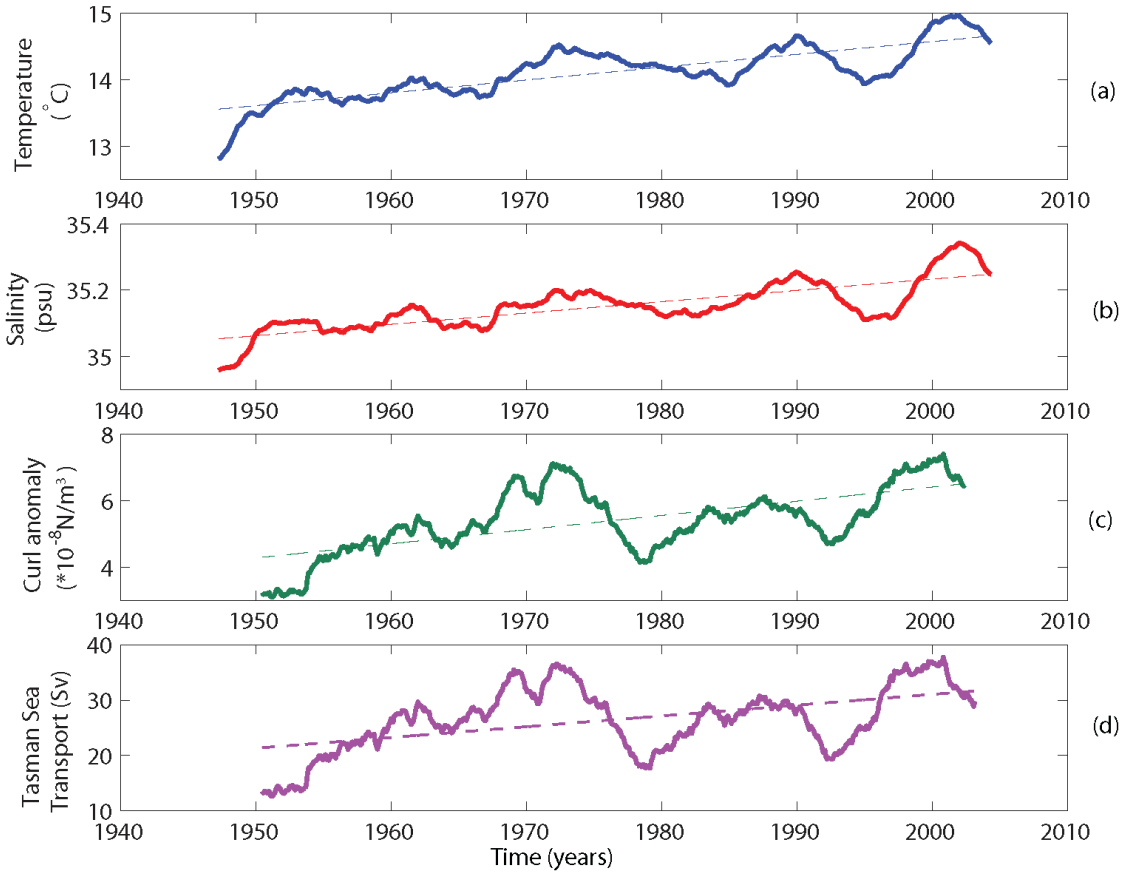

Figure 13.15

Low-pass filtered time series of (a) SST (in °C) and (b) salinity (in psu) at the Maria Island coast station, (c) South Pacific regional mean wind stress curl (in N m^{-3}; 20–50°S, 180–80°W), and (d) net volume transport (in Sv) through the Tasman Sea, calculated using Godfrey's Island Rule. Dashed lines show the linear trend. Adapted from Hill et al. (2008).